

# 1 Detailed budget analysis of HONO in central London 2 reveals a missing daytime source

3 J. D. Lee<sup>1,2</sup>, L. K. Whalley<sup>3,4</sup>, D. E. Heard<sup>3,4</sup>, D. Stone<sup>4</sup>, R. E. Dunmore<sup>2</sup>, J. F.  
4 Hamilton<sup>2</sup>, D. E. Young<sup>5,\*</sup>, J. D. Allan<sup>5,6</sup>, S. Laufs<sup>7</sup> and J. Kleffmann<sup>7</sup>.

5 [1] National Centre for Atmospheric Science, WACL Building, University of York, York,  
6 UK.

7 [2] Department of Chemistry, University of York, York, UK.

8 [3] National Centre for Atmospheric Science, University of Leeds, Leeds, UK.

9 [4] School of Chemistry, University of Leeds, Leeds, UK.

10 [5] School of Earth, Atmospheric and Environmental Sciences, University of Manchester,  
11 Oxford Road, Manchester, M13 9PL, UK.

12 [6] National Centre for Atmospheric Science, University of Manchester, Oxford Road,  
13 Manchester, M13 9PL, UK.

14 [7] Physikalische und Theoretische Chemie / Fakultät Mathematik und Naturwissenschaften,  
15 Bergische Universität Wuppertal (BUW), Gaußstr. 20, 42119 Wuppertal, Germany.

16 \*now at: Department of Environmental Toxicology, University of California, Davis, CA  
17 95616, USA.

18 Correspondence to: J. D. Lee (james.lee@york.ac.uk)

19

## 20 Abstract

21 Measurements of HONO were carried out at an urban background site near central London as  
22 part of the *Clean air for London* (ClearfLo) project in summer 2012. Data was collected from  
23 22<sup>nd</sup> July – 18<sup>th</sup> August 2014, with peak values of up to 1.8 ppbV at night and non-zero values  
24 of between 0.2 and 0.6 ppbV seen during the day. A wide range of other gas phase, aerosol,  
25 radiation and meteorological measurements were made concurrently at the same site, allowing  
26 a detailed analysis of the chemistry to be carried out. The peak HONO / NO<sub>x</sub> ratio of 0.04 is  
27 seen at ~02:00 UTC, with the presence of a second, daytime peak in HONO / NO<sub>x</sub> of similar  
28 magnitude to the night-time peak suggesting a significant secondary daytime HONO source.

1 A photostationary state calculation of HONO involving formation from the reaction of OH  
2 and NO and loss from photolysis, reaction with OH and dry deposition shows a significant  
3 underestimation during the day, with calculated values being close to zero, compared to the  
4 measurement average of 0.4 ppbV at midday. The addition of further HONO sources from the  
5 literature, including dark conversion of NO<sub>2</sub> on surfaces, direct emission, photolysis of ortho-  
6 substituted nitro phenols, the postulated formation from the reaction of HO<sub>2</sub>×H<sub>2</sub>O with NO<sub>2</sub>,  
7 photolysis of adsorbed HNO<sub>3</sub> on ground and aerosols, and HONO produced by  
8 photosensitized conversion of NO<sub>2</sub> on the surface increases the daytime modelled HONO to  
9 0.1 ppbV, still leaving a significant missing daytime source. The missing HONO is plotted  
10 against a series of parameters including NO<sub>2</sub> and OH reactivity (used as a proxy for organic  
11 material), with little correlation seen. Much better correlation is observed with the product of  
12 these species with j(NO<sub>2</sub>), in particular NO<sub>2</sub> and the product of NO<sub>2</sub> with OH reactivity. This  
13 suggests the missing HONO source is in some way related to NO<sub>2</sub> and also requires sunlight.  
14 Increasing the photosensitized surface conversion rate of NO<sub>2</sub> by a factor of 10 to a mean  
15 daytime first order loss of ~6 x 10<sup>-5</sup> s<sup>-1</sup> (but which varies as a function of j(NO<sub>2</sub>)) closes the  
16 daytime HONO budget at all times (apart from the late afternoon) suggesting that urban  
17 surfaces may enhance this photosensitized source. The effect of the missing HONO to OH  
18 radical production is also investigated and it is shown that the model needs to be constrained  
19 to measured HONO in order to accurately reproduce the OH radical measurements.

20

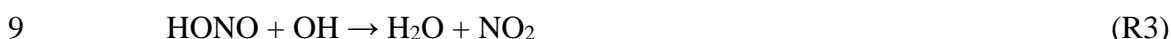
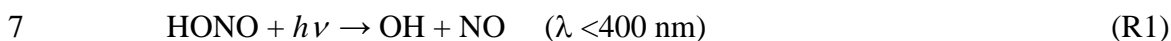
## 21 **1 Introduction**

22 The hydroxyl radical (OH) is the main daytime oxidant in the troposphere, playing a key role  
23 in the chemical transformations of trace species (Levy II, 1971). A major source of OH,  
24 especially in polluted environments, is the photolysis of nitrous acid (HONO) in the near UV  
25 region (R2). It has been shown in numerous studies that HONO can actually be the dominant  
26 early morning source of OH (Ren et al., 2003; Ren et al., 2006; Dusanter et al., 2009;  
27 Michoud et al., 2012) and has often been shown to also be significant during the rest of the  
28 day (Elshorbany et al., 2009; Hofzumahaus et al., 2009; Villena et al., 2011; Michoud et al.,  
29 2014). This is mainly due to unexpectedly high levels of HONO measured during daylight  
30 hours when fast photolysis would have been expected to keep concentrations low and hence  
31 insignificant for a source of OH. As a result of these studies, it has become clear that HONO

1 has the ability to initiate and accelerate daytime photochemistry and hence knowledge of its  
2 formation and loss are crucial to understanding tropospheric oxidation chemistry.

3 Typically, HONO in the troposphere would be expected to be governed by formation by the  
4 reaction between nitric oxide (NO) and OH (R2) and losses by photolysis (R1) and oxidation  
5 by OH (R3).

6



10

11 These reactions can be used, along with measurements of concentrations of the relevant  
12 species and HONO photolysis rates, to calculate a photochemical steady state concentration  
13 of HONO. Such calculations from field studies typically show a peak of HONO at night  
14 (when there is no photolysis), with levels in the low pptv range during the day. However,  
15 measurements usually show that daytime HONO levels can reach substantially higher  
16 concentrations than this, with mixing ratios up to a few hundred pptv frequently observed  
17 (Zhou et al., 2002; Kleffmann et al., 2005; Acker et al., 2006). It is clear from these analyses  
18 that there is an extra source of HONO present, which can have a significant impact on the  
19 atmospheric oxidising capacity due to its potential to form OH. A range of reactions have  
20 been postulated during the various studies to account for the missing source of HONO, with  
21 these likely to be heterogeneous either on aerosols or the ground itself. Major ground surfaces  
22 were recently confirmed by direct flux measurements of HONO (Ren et al., 2011; Zhou et al.,  
23 2011; Zhang et al., 2012). Tower measurements (Harrison and Kitto, 1994; Kleffmann et al.,  
24 2003; Oswald et al., 2015; Sörgel et al., 2011a, 2015; Stutz et al., 2002; Vandenkoer et al.,  
25 2013; Villena et al., 2011; Vogel et al., 2003; Wong et al., 2012; Young et al., 2012), and  
26 aircraft observations (Li et al., 2014; Zhang et al., 2009) have also demonstrated that major  
27 HONO sources exist at canopy or ground surfaces through the measurement of vertical  
28 gradients. It is postulated that such processes involve the conversion of nitrogen dioxide  
29 (NO<sub>2</sub>) or nitric acid (HNO<sub>3</sub>) to HONO on ground surfaces and are enhanced by sunlight, thus  
30 providing a daytime only source of HONO (Zhou et al., 2003; George et al., 2005). In  
31 addition, bacterial production of nitrite in soil surfaces were also proposed as additional

1 HONO source (Su et al., 2011, Oswald et al., 2013). It has also been shown that HONO is  
2 emitted directly from petrol and diesel vehicle exhausts (Kurtenbach et al., 2001; Li et al.,  
3 2008). At most sites, this is a relatively small contributor to HONO due to its relatively short  
4 atmospheric lifetime in the daytime (10-20 minutes), however close to major roads and  
5 especially in tunnels in can contribute greatly to the HONO present. A recent publications by  
6 Michoud et al. (2014) gives a good summary of the possible daytime HONO sources under  
7 similar conditions to this study (in Paris) and a reivew by Kleffmann (2007) also discusses  
8 daytime HONO sources in depth.

9 Almost all previous field studies still show a significant missing daytime HONO source, thus  
10 showing the requirement for more studies. In this work we report what are, to our knowledge,  
11 the first measurements of HONO made in London, UK, one of the largest cities in Europe.  
12 The measurements were made as part of the summer intensive operation period of the *Clean*  
13 *Air for London* (ClearfLo) project and, as a result, were made concurrently with a wide range  
14 of other atmospheric gas and aerosol phase species (including OH, HO<sub>2</sub>, NO, NO<sub>2</sub> and  
15 photolysis rates). This has enabled us to undertake a detailed modelling study of HONO using  
16 the Master Chemical Mechanism (MCMv3.2), in which we have included a series of known  
17 sources of HONO found in the literature. We then investigate the difference between daytime  
18 measured and modelled HONO, with a simple correlation analysis against other measured  
19 parameters. The model was also used to assess the radical forming potential of the missing  
20 HONO, which can ultimately lead to increased production of secondary pollutants such as  
21 ozone (O<sub>3</sub>) and secondary organic aerosol (SOA).

22

## 23 **2 Experimental**

24 The ClearfLo project had the aim of providing an integrated measurement and modelling  
25 program in order to help better understand the atmospheric processes that affect air quality  
26 (Bohnenstengel et al., 2014). As part of ClearfLo, a summer intensive operation period (IOP)  
27 took place in July and August 2012, which involved the measurement of a wide range of gas  
28 and aerosol phase species (including meteorology), which enabled a detailed study of the  
29 atmospheric chemistry of London's air to be carried out.

30

### 31 **2.1 Site description**

1 The main site for the IOP was an urban background site at the Sion Manning School in North  
2 Kensington, London, ( $51^{\circ} 31' 16''$  N,  $0^{\circ} 12' 48''$  W), which is situated in a residential area  
3 approximately 7 km west of central London (defined here as Oxford Street). Measurements of  
4 NO, NO<sub>2</sub> and total reactive nitrogen (NO<sub>y</sub>), sulphur dioxide (SO<sub>2</sub>), O<sub>3</sub>, carbon monoxide  
5 (CO), PM<sub>10</sub> and total particle number concentration have been routinely made at the site  
6 since January 1996 as part of the Automatic Urban and Rural Network (AURN) and the  
7 London Air Quality Network (LAQN) (Bigi and Harrison, 2010). For the ClearLo IOP, other  
8 instruments were installed in various shipping container laboratories in the grounds of the  
9 school, all within 20 metres of the long term measurements. A full description of the  
10 campaign, including the instruments present can be found in (Bohnenstengel et al., 2014),  
11 however details of the measurements pertinent to this work are given below. All  
12 measurements were carried out at a height of around 5 metres above ground level, within a  
13 horizontal area of 10 metres from each other.

14

## 15 **2.2 HONO measurements**

16 HONO was measured using a long-path absorption photometer (LOPAP) instrument from the  
17 University of Wuppertal, Germany, which is explained in detail elsewhere (Heland et al.,  
18 2001). Briefly, gaseous HONO is sampled in a stripping coil containing a mixture of  
19 sulfanilamide in a 1M HCl solution and is derivatized into an azo dye. The light absorption by  
20 the azo dye is measured in a long path absorption tube by a spectrometer at 550 nm using an  
21 optical path length of 2.4 m. The stripping coil was placed directly in the atmosphere being  
22 sampled; meaning the length of the glass inlet was only 2 cm minimizing sampling artefacts.  
23 The LOPAP has two stripping coils connected in series to correct interferences. In the first  
24 coil (channel 1), HONO is trapped quantitatively together with a small amount of the  
25 interfering substances. Assuming that these interfering species are trapped in a similar amount  
26 in the second coil (channel 2), the difference between the signals of the two channels provides  
27 an interference-free HONO signal. Zero measurements were performed every 7 hours.  
28 Calibrations of the spectrometer using a known concentration of the derivatized azo dye were  
29 carried out 3 times during the campaign. The instrument was previously successfully  
30 validated against the spectroscopic DOAS technique under urban conditions and in a smog  
31 chamber (Kleffmann et al., 2006). During the campaign a detection limit of 1 pptV (for a time  
32 resolution of 5 min), a precision of 1 % and an accuracy of 10 % were obtained.

1

## 2 **2.3 Radical measurements**

3 OH, HO<sub>2</sub> and RO<sub>2</sub> radical concentrations were measured using the FAGE (fluorescence assay  
4 by gas expansion) technique (Heard and Pilling, 2003). In the case of HO<sub>2</sub> and RO<sub>2</sub>, the  
5 radicals were first titrated with NO to OH before FAGE detection. The current mode of  
6 operation is described in detail elsewhere (Whalley et al., 2015a). The HO<sub>2</sub> observations used  
7 as a constraint in the modelling studies reported in section 3.3 were made using a low flow of  
8 NO (7.5 sccm), which laboratory tests have shown minimised interferences from alkene and  
9 aromatic-derived RO<sub>2</sub> species (Whalley et al., 2013). Under this regime, the interference from  
10 RO<sub>2</sub> radicals present is estimated to contribute <3 % to the HO<sub>2</sub> concentration. The limit of  
11 detection (LOD) at a signal to noise ratio of three for one data acquisition cycle was ~1.3 x  
12 10<sup>6</sup> molecule cm<sup>-3</sup> for OH and ~6.3×10<sup>6</sup> molecule cm<sup>-3</sup> for HO<sub>2</sub>. The measurements were  
13 recorded with 1 s time-resolution, and the accuracy of the measurements was ~15 %.

14

## 15 **2.4 Other supporting measurements**

16 The NO and NO<sub>2</sub> data used in this work were taken using an Air Quality Design Inc. custom  
17 built high sensitivity chemiluminescence analyser with LED based blue light NO<sub>2</sub> converter.  
18 The instrument consists of two channels measuring NO by reaction with excess O<sub>3</sub> to form  
19 excited state NO<sub>2</sub> followed by the detection of the resultant chemiluminescence (Drummond  
20 et al., 1985; Lee et al., 2009). The air flow in one of the channels first passes through a  
21 photolytic converter where light at 395 nm from an array of LEDs photolyses NO<sub>2</sub> to NO.  
22 The 395 nm wavelength has a specific affinity for NO<sub>2</sub> photolytic conversion to NO, giving  
23 high analyte selectivity within the channel and there is a low probability of other species  
24 (such as HONO) being photolysed (Pollack et al., 2010). This makes this measurement a  
25 significant improvement over the high temperature catalytic NO<sub>2</sub> conversion used for the long  
26 term measurement at the North Kensington site (Steinbacher et al., 2007; Villena et al., 2012).  
27 Calibration of the instrument was carried out every 2 days using 5 ppm NO in nitrogen (BOC  
28 – certified to NPL scale) - diluted to ~20 ppb using high purity zero air (BOC BTCA 178).  
29 The NO<sub>2</sub> conversion efficiency (ca. 40%) was calibrated using gas phase titration of the NO  
30 standard by O<sub>3</sub>. NO<sub>y</sub> data were taken using a TEI 42i TL NO analyser with Molybdenum  
31 converter.

1 VOC measurements were obtained using two gas chromatography (GC) instruments. The  
2 volatile fraction of VOCs (C<sub>2</sub>-C<sub>7</sub> hydrocarbons, with a small selection of OVOCs) was  
3 measured using a dual channel (DC)-GC-FID (flame ionization detector) (Hopkins et al.,  
4 2003), while a comprehensive two dimensional GC (GC×GC-FID) measured the less volatile  
5 fraction (C<sub>6</sub>-C<sub>13</sub>, with a large group of OVOCs) (Lidster et al., 2014).

6 Measurements of HCHO were made using an Aerolaser 4021 analyser (Salmon et al., 2008).  
7 Briefly, gaseous formaldehyde is scrubbed into the liquid phase via a stripping coil containing  
8 dilute sulphuric acid. This is followed by reaction with Hantzsch reagent, a dilute solution  
9 made with acetyl acetone, acetic acid, and ammonium acetate. Aqueous phase formaldehyde  
10 reacts with this reagent via the ‘Hantzsch reaction’ to produce 3,5-diacetyl-1,4-  
11 dihydrolutidine (DDL). Once excited by an appropriate wavelength (400 nm in this case),  
12 DLL fluoresces thus allowing quantitative assay by monitoring the emitted light.

13 Non-refractory PM<sub>1.0</sub> nitrate, sulphate, organic matter, chloride and ammonium were  
14 quantified using a compact time-of-flight aerosol mass spectrometer (cToF-AMS - Aerodyne  
15 Inc.), which gave data with a time resolution of 5 minutes (Young et al., 2015). Ammonium is  
16 reflective of the overall ammonium nitrate because ammonium nitrate is both non-refractory  
17 and tends to be in the submicron fraction. While there is supermicron nitrate, it is  
18 overwhelmingly in the form of sodium nitrate, which is refractory and not measured by the  
19 AMS. It is specifically the nitrate measurement that is of interest here because it pertains to  
20 the working hypothesis.

21 Total aerosol surface area was calculated using data from an aerodynamic particle sizer (APS)  
22 instrument (TSI Inc, model 3321). The mean diameter of particles in each size bin (assume  
23 spherical) multiplied number of particles in that bin. In total there were 53 size bins ranging  
24 from 0.53 to 21.29 μm. Actinic fluxes of solar radiation were measured using a spectral  
25 radiometer, which consisted of an Ocean Optics high resolution spectrometer (QE65000),  
26 couple via fibre optic to a 2π quartz collection dome. These measurements were then used to  
27 calculate the photolysis frequencies of a number of >50 trace gases, including NO<sub>2</sub>, HONO  
28 and O<sub>3</sub> ( $j(O^1D)$ ) (Kraus and Hofzumahaus, 1998; Edwards and Monks, 2003). Wind speed  
29 and direction, temperature and relative humidity were measured using a Davis Vantage Vue  
30 met station. Mixing heights estimation was based on the vertical profiles of the hourly vertical  
31 velocity variance (Barlow et al., 2011). The vertical velocity variance was measured with a  
32 Doppler Lidar (Halo-Photonics scanning Doppler lidar) located at the North Kensington site

1 with a gate resolution of 18 m; the un-sampled portion of the vertical velocity variance is  
2 calculated with the spectral correction technique described in (Barlow et al., 2015). The  
3 mixing height is defined as the height up to which the vertical velocity variance is higher than  
4  $0.1 \text{ m}^2 \text{ s}^{-2}$ . This threshold value was perturbed by 20%, (i.e. between  $0.08 \text{ m}^2 \text{ s}^{-2}$  and  $0.121 \text{ m}^2$   
5  $\text{s}^{-2}$ ) and the median of the estimated values was taken as the hourly mixing height.

6

## 7 **3 Results**

### 8 **3.1 Overview of data**

9 Data were collected from 22<sup>nd</sup> July – 18<sup>th</sup> August 2012 and time series of local wind speed,  
10 wind direction, NO, NO<sub>2</sub>, O<sub>3</sub>, HONO and the photolysis rate of HONO ( $j(\text{HONO})$ ) are shown  
11 in figure 1. The majority of the measurement period was characterised by south westerly  
12 winds, with the wind speed showing a diurnal cycle of less than  $1 \text{ m s}^{-1}$  at night (the minimum  
13 measurable by the anemometer) to  $4 - 6 \text{ m s}^{-1}$  in late afternoon. These periods show NO and  
14 NO<sub>2</sub> with peaks of 15 ppbV and 10 ppbV respectively, typically at ~07:30 UTC, the peak of  
15 the morning rush hour. O<sub>3</sub> shows a diurnal cycle with a typical maximum of  $40 - 45 \text{ ppbV}$  at  
16 ~16:00 UTC and minima of  $<20 \text{ ppbV}$  at night. The exceptions to this are two periods from  
17 24<sup>th</sup> – 27<sup>th</sup> July and 8<sup>th</sup> – 10<sup>th</sup> August, during which the site was subjected to generally easterly  
18 flow, with lower wind speed. Due to central London being to the East of the site, these  
19 periods are characterised by higher levels of NO<sub>x</sub> (up to  $60 \text{ ppbV}$  of NO and  $50 \text{ ppbV}$  of  
20 NO<sub>2</sub>), which has its source mainly from traffic exhaust. O<sub>3</sub> is also higher during these periods,  
21 due to a combination of the higher primary pollution levels (NO<sub>x</sub> and VOCs) and low wind  
22 speeds causing a build-up of this secondary pollutant during the 3-4 day period. Peak daytime  
23 levels of O<sub>3</sub> of  $60 - 100 \text{ ppbV}$  are observed during these more polluted periods. HONO  
24 concentrations show peak values at night throughout the campaign (up to  $1.8 \text{ ppbV}$  during the  
25 easterly periods and up to  $0.7 \text{ ppbV}$  during the rest of the campaign), with non-zero values  
26 seen during the day ( $0.3 - 0.6 \text{ ppbV}$ ).

27 This behaviour is better visualised using the average diurnal cycle, which is shown for HONO  
28 and NO<sub>x</sub> in figure 2(a) and  $j(\text{HONO})$  and the HONO / NO<sub>x</sub> ratio in figure 2(b). As well as the  
29 total campaign average, diurnal cycles are shown for the easterly and westerly time periods  
30 described above. NO<sub>x</sub> follows an expected profile, with a peak of  $29 \text{ ppbV}$  on average during  
31 the morning rush hour at ~05:30 UTC (06:30 local time), followed by a decrease during the  
32 day, due largely to increasing boundary layer depth and hence dilution. After ~16:00 UTC,

1 the  $\text{NO}_x$  levels begin to rise from a minimum of 8.5 ppbV, due to a combination of increased  
2 emissions during the evening rush hour and the reduction of the boundary layer depth into the  
3 night. Concentrations reach  $\sim 18$  ppbV by midnight and remain reasonably constant  
4 throughout the rest of the night. Diurnal averages in the easterly and westerly conditions  
5 follow the same pattern as for the total data series, with significantly higher  $\text{NO}_x$  during the  
6 easterly period. During the morning peak,  $\text{NO}_x$  is a factor of 3 higher during easterly flow  
7 compared to westerly and 15 - 20 % higher during the daytime. HONO appears to follow a  
8 similar diurnal profile to  $\text{NO}_x$ , which is not unexpected since the main known HONO sources  
9 involve nitrogen oxides. However, the morning peak of HONO is around 1 hour earlier  
10 compared to  $\text{NO}_x$  (at around 04:30) due to the onset of HONO photolysis at sunrise. HONO  
11 concentrations are also higher under easterly flow conditions compared to westerly, with the  
12 early morning peak being a factor of around 2 higher and the daytime average around 25%  
13 higher. The behaviour of HONO is perhaps better described by looking at the  $\text{HONO} / \text{NO}_x$   
14 ratio and the average diurnal cycle of  $\text{HONO} / \text{NO}_x$  and  $j(\text{HONO})$  is shown in figure 2b. The  
15 peak  $\text{HONO} / \text{NO}_x$  of 0.04 is seen at  $\sim 02:00$  UTC, due to the lack of photolysis (the major  
16 loss route for HONO), direct HONO emissions and heterogeneous HONO formation at the  
17 surface during the night, into a relatively shallow boundary layer. After this (and before  
18 sunrise), the ratio begins to decrease due to the onset of fresh  $\text{NO}_x$  emissions and continues to  
19 decrease during the morning due to the increase of HONO photolysis. If the HONO sources  
20 which are active during night-time are the only active sources also during daytime, the  
21  $\text{HONO}/\text{NO}_x$  ratio should show a deep minimum around noon. In contrast, in figure 2 a  
22 maximum is observed, which is a hint to an additional daytime source. In addition, the  
23 maximum of  $\text{HONO}/\text{NO}_x$  correlates well with the radiation, which is again a hint for a  
24 photochemical process.

25 The HONO levels measured in London are within the range of data published from other  
26 urban sites, although there is a wide range of concentrations reported in the literature.  
27 Michoud et al., 2014 reported daytime levels of 0.11 ppbV (averaged for 3 hours around local  
28 solar noon) at a site near Paris, France, which is lower than our value of 0.44 ppbV. However  
29 the site was 14 km from the centre of Paris (upwind), significantly further away from the  
30 major emission sources than the London site. As a result,  $\text{NO}_x$  was lower in Paris, with a  
31 daytime campaign average of 5.3 ppbV compared to our value of 13.9 ppbV, giving a daytime  
32  $\text{HONO} / \text{NO}_x$  ratio of 0.020 compared to our value of 0.031, although this may be partially  
33 explained by the lower  $j(\text{HONO})$  values in London compared to Paris. The fact that the

1 London site is closer to emission sources will most likely also influence this, as direct  
2 emission of HONO from traffic exhaust is potentially a significant proportion of HONO in  
3 large cities (Kurtenbach et al., 2001). Kleffmann et al, 2006, reported daytime HONO levels  
4 of between 0.2 – 0.3 ppbv in Milan, Italy. They also compared data from a LOPAP instrument  
5 (similar to that used in this study) and a Differential Optical Absorption Spectroscopy  
6 (DOAS) instrument and showed excellent agreement. The resultant HONO / NO<sub>x</sub> ratio  
7 reported was 0.046. Wong et al., 2012, reported daytime HONO mixing ratios averting 0.1  
8 ppbv in Houston, USA, with corresponding average daytime NO<sub>x</sub> of 10 ppbv, giving a HONO  
9 / NO<sub>x</sub> ratio of 0.03. Some other studies in large cities have reported larger daytime HONO  
10 concentrations, e.g. Santiago, Chile (1.5 ppbV) (Elshorbany et al., 2009), Guangzhou, China  
11 (2.0 ppbV) (Qin et al., 2009) and Xinken, China (0.80 ppbV) (Su et al., 2008a; Su et al.,  
12 2008b), however, all of these were at sites with much larger NO<sub>x</sub> loading and so the resultant  
13 HONO / NO<sub>x</sub> ratio is similar to the measurements in London. The range of ambient HONO  
14 values reported in the literature suggest that the specific conditions at a particular site are key  
15 to the HONO levels, in particular the prevalence of different levels of NO<sub>x</sub> during daylight  
16 hours. Thus a modelling study including a range of known HONO sources and sinks is  
17 required to fully understand the observed behaviour.

18

### 19 **3.2 HONO photostationary state approach**

20 In order to initially assess HONO concentrations and in particular the impact of any potential  
21 extra sources during this campaign, a photostationary state (PSS) calculation has been carried  
22 out. In this approach, the sources and sinks of the species in question are assumed to balance  
23 each other and is thus only suitable for species with a short lifetime, such as free radicals.  
24 However, it has been widely used to study the daytime HONO budget, despite its lifetime  
25 being in the range of 10 – 20 minutes during the day (Alicke et al., 2002; Wong et al., 2012),  
26 resulting in significant uncertainties, especially for measurements close to emission sources  
27 (Lee et al., 2013). However, the measurement site in this study is described as an urban  
28 background site and thus is relatively free from the influence of major roads or point sources.  
29 Calculation of the transport time since emission using the NO<sub>x</sub> / NO<sub>y</sub> ratio (using the  
30 technique described in (Cappa et al., 2012)) shows a lifetime since emission of 40-50 minutes,  
31 significantly greater than the photochemical lifetime of HONO (typically 10 - 20 minutes at  
32 noon). Thus, we consider the PSS approach still as a useful tool to quantify HONO sources

1 during daytime. HONO is expected to be in photostationary state due to its formation by the  
2 reaction between OH and NO, and its sinks by rapid photolysis (to reform OH and NO), its  
3 reaction with OH and its dry deposition. Combining these terms, the concentration  
4  $[\text{HONO}]_{\text{PSS}}$  can be calculated using the following equation (1):

5

$$6 \quad \text{HONO}_{\text{PSS}} = \frac{k_{\text{OH}+\text{NO}}[\text{OH}][\text{NO}]}{k_{\text{OH}+\text{HONO}}[\text{OH}] + j(\text{HONO}) + \frac{v_{\text{HONO}}}{h}} \quad (1)$$

7

8 Measured data were used for OH, NO and  $j(\text{HONO})$ , with the relevant pressure and  
9 temperature dependant rate constants for  $k_{\text{OH}+\text{NO}}$  and  $k_{\text{OH}+\text{HONO}}$  taken from (Atkinson et al.,  
10 2004).  $v_{\text{HONO}}$  is the deposition velocity of HONO, set at an upper limit of  $3.0 \text{ cm s}^{-1}$ , and  $h$  is  
11 the boundary layer height. We use an effective HONO boundary layer height (BL) of 75 m,  
12 calculated using typical Eddy diffusion coefficients and  $j(\text{HONO})$ , as the likely height to  
13 which HONO will reach, given a daytime lifetime of 15 minutes. This method will strongly  
14 underestimate HONO deposition because the boundary layer height will be considerably  
15 larger than the height at which HONO will actually be transported to, due to its short lifetime  
16 (10-20 minutes during the day). This effect is partly compensated for by using  $3.0 \text{ cm s}^{-1}$  for  
17 the deposition velocity, which is at the upper end of the ranges quoted in the literature  
18 (Harrison and Kitto, 1994; Stutz et al., 2002; Trebs et al., 2006); however it does mean there  
19 are considerable errors in this approach. The PSS analysis also does not consider vertical  
20 structure, thus the magnitude of any unknown source inferred from the analysis will be  
21 dependent on the height above the ground surface that the measurements are being made. The  
22 average daytime diurnal profiles in both easterly and westerly conditions are shown in figure  
23 3. We do not consider night time data as the PSS approach would not be valid at night. We  
24 only consider data from 08:00 UTC ( $j(\text{HONO}) > 4 \times 10^{-4} \text{ s}^{-1}$ ), a time at which all HONO  
25 produced during the night will have been lost due to photolysis after sunrise. It is clear that  
26 the PSS calculation cannot replicate the measured HONO during daylight hours (08:00 –  
27 20:00 UTC). The PSS does appear to reproduce the daylight cycle of HONO, with high  
28 concentrations during the morning peak between 06:00 and 09:00, due to the increase in NO  
29 and OH at the morning rush hour. However, after this morning peak,  $\text{HONO}_{\text{PSS}}$  rapidly  
30 decreases to  $< 0.05 \text{ ppbV}$  by midday, followed by a gradual decrease during the afternoon  
31 reaching a minimum of  $0.007 \text{ ppbv}$  at 19.30. This is due to the rapid photolysis of HONO,

1 which occurs in the near UV region, and occurs significantly faster than the only production  
2 route in the PSS calculation (OH + NO), especially during the later part of the day when NO  
3 is low. HONO<sub>PSS</sub> during the day shows similar levels in both easterly and westerly conditions,  
4 despite measured HONO being significantly higher in the more polluted easterly regime. The  
5 PSS treatment of HONO is clearly incomplete, with significant missing source terms.

6

### 7 **3.3 HONO box model approach**

8 In order to assess the importance of other potential HONO sources in our study, we use a  
9 photochemical model based on the Master Chemical Mechanism (MCMv3.2) (Jenkin et al.,  
10 2012). Complete details of the kinetic and photochemical data used in the mechanism are  
11 available at the MCM website (<http://mcm.leeds.ac.uk/MCM/home>). The model was run with  
12 a sub-set of the MCM and treated the degradation of simultaneously measured trace VOCs,  
13 CH<sub>4</sub> and CO following oxidation by OH, O<sub>3</sub> and NO<sub>3</sub> and included ~15,000 reactions and  
14 ~3,800 species. The model was constrained to measurements of NO, NO<sub>2</sub>, O<sub>3</sub>, CO, CH<sub>4</sub>, 62  
15 individual VOC species measured by GC-FID and also 2D-GC, PAN, HCHO, HNO<sub>3</sub>, HO<sub>2</sub>,  
16 water vapour, temperature and pressure. The model was constrained with the measured  
17 photolysis rates (including  $j(O^1D)$ ,  $j(NO_2)$ ,  $j(HONO)$ ,  $j(HCHO)$ ,  $j(CH_3COCH_3)$  and  
18  $j(CH_3CHO)$ ). A constant H<sub>2</sub> concentration of 500 ppbV was assumed (Forster et al., 2012).  
19 The model inputs were updated every 15 minutes. For species measured more frequently, data  
20 was averaged to 15 minute intervals, whilst those measured at a lower time resolution were  
21 interpolated. The loss of all non-constrained, model generated, species by a wind speed  
22 dependent deposition ( $v$ ) was calculated by summing the resistances  $1/R_a$ ,  $1/R_b$  and  $1/R_c$ , for  
23 which  $R_a$  describes turbulent convective transport,  $R_b$  the laminar diffusion near the surface  
24 and  $R_c$  the surface resistance. The inverse of the surface resistances ( $1/R_c$ ) assumed are 3 cm  
25 s<sup>-1</sup> for HNO<sub>3</sub> and 2 cm s<sup>-1</sup> for HONO and 1 cm s<sup>-1</sup> for NO<sub>2</sub> (and all other non-constrained  
26 model species). For the campaign average wind speed of 1.6 m s<sup>-1</sup>,  $v_{HNO_3}$ ,  $v_{HONO}$  and  $v_{NO_2}$   
27 equal 0.52, 0.48 and 0.38 cm s<sup>-1</sup> respectively. As with the steady state approach, we use an  
28 effective HONO boundary layer height (BL) of 75 m in the model. This assumption leads to a  
29 campaign average first order loss of HONO (at a mean wind speed of 1.6 m s<sup>-1</sup>) of  $v_{HONO}/BL$   
30 =  $6.4 \times 10^{-5}$  s<sup>-1</sup>. The model was run for the entirety of the campaign in overlapping 7 day  
31 segments. To allow all the unmeasured, model generated intermediate species time to reach  
32 steady state concentrations, the model was initialised with inputs from the first measurement

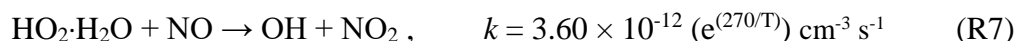
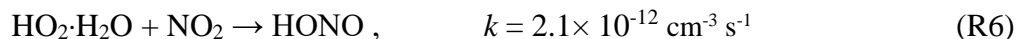
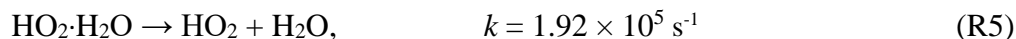
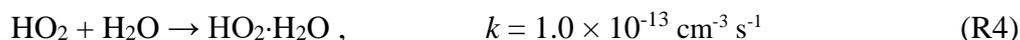
1 day (22<sup>nd</sup> July) for 5 days before comparison to measurements were made. Comparison of  
2 these 5 spin up days demonstrated that the concentration of model generated species rapidly  
3 converged and there was less than a 1% difference in (for example) modelled OH or HONO  
4 concentration by the second spin up day. As a result of this, the model segments were run so  
5 as to overlap for 2 days only to reduce the computing time. The model was run unconstrained  
6 to HONO (for the results presented in this paper) for comparison with measured HONO  
7 concentration.

8 A number of HONO sources in addition to the gas phase source from the reaction of hydroxyl  
9 radicals with NO have been included in the model. These include:

10 a.) A direct emission source of HONO was added to the model, using a ratio of HONO:NO<sub>x</sub>  
11 of 0.008 reported previously from tailpipe emission studies of NO<sub>x</sub> and HONO in a tunnel  
12 (Kurtenbach et al., 2001) and the measured NO<sub>x</sub> concentrations. It is likely that the used  
13 value represents an upper limit of the direct emission contribution to HONO during  
14 daytime, due to the short atmospheric lifetime of HONO (10-20 minutes) compared to  
15 NO<sub>x</sub>.

16 b.) It has been suggested that a reaction between HO<sub>2</sub>·H<sub>2</sub>O and NO<sub>2</sub> could produce HONO at  
17 a sufficiently fast rate to be a significant source in the troposphere (Li et al., 2014). It had  
18 previously been shown in laboratory studies that this reaction produces negligible HONO  
19 yields under dry conditions (Tyndall et al., 1995; Dransfield et al., 2001). However, in the  
20 lower troposphere, around 30% of HO<sub>2</sub> is suggested to be present as an HO<sub>2</sub>·H<sub>2</sub>O complex,  
21 and hence may show different chemical behaviour. Kinetic measurements of the self  
22 reaction HO<sub>2</sub> + HO<sub>2</sub> have revealed the chaperone effect of water vapour enhancing the rate  
23 coefficient (Stone et al., 2005). It has also been shown that the rate coefficient of the  
24 reaction HO<sub>2</sub>+NO<sub>2</sub> increase by 50% from dry to humid atmospheric conditions (Sander  
25 and Peterson, 1984). In the Li et al. study it was postulated that the reaction converts NO<sub>2</sub>  
26 to HONO with a yield of 100% and this allowed a model to reproduce the observed levels  
27 of HONO, albeit under free tropospheric conditions away from surfaces. Inclusion of this  
28 reaction also improved the agreement between the model and measured levels of HO<sub>2</sub> and  
29 NO<sub>x</sub>. However, recent field data has shown that in fact, this reaction produces only a 3%  
30 yield of HONO (Ye et al., 2015), thus greatly reducing the impact of the reaction on  
31 HONO production. Nevertheless, the following additional reactions were included in our  
32 MCM model to account for the equilibrium that exists between uncomplexed and H<sub>2</sub>O-

1 complexed HO<sub>2</sub> in the atmosphere (R4 & R5) and the major reactions of H<sub>2</sub>O-complexed  
2 HO<sub>2</sub> in this urban environment (R6 and R7):



8  
9 c.) Light induced heterogeneous conversion of NO<sub>2</sub> to HONO on aerosol surfaces was also  
10 considered assuming an uptake coefficient of 10<sup>-6</sup> (Kleffmann et al., 1999; Arens et al.,  
11 2001; Monge et al., 2010).

12 d.) Heterogeneous conversion of NO<sub>2</sub> to HONO on ground surfaces at a rate equal to ~2×10<sup>-8</sup>  
13 s<sup>-1</sup> has been included in the model which is consistent with laboratory studies, which put an  
14 upper limit on dark surface source of <10<sup>-7</sup>, e.g. Stemmler et al. (2007). This was  
15 parameterised in the model by taking the wind-speed dependent  $\nu_{\text{NO}_2}$  and assuming  
16 instantaneous mixing of surface emitted HONO up to a height of 75 m. This leads to a first  
17 order loss of NO<sub>2</sub> to the ground at a rate of 4 x 10<sup>-5</sup> s<sup>-1</sup> on average. This rate was scaled  
18 down by a factor of 2000 to represent the dark surface conversion of NO<sub>2</sub> to HONO  
19 reported in laboratory studies. However, it has to be stressed, that the present calculation  
20 strongly underestimates the contribution of heterogeneous HONO formation on ground  
21 surfaces, especially during night-time at the measurement height, caused by the assumption  
22 of an instantaneous mixing up to a height of 75 m, see Eq 1.

23 e.) A daytime source from the photolysis of ortho nitro phenols which were not measured  
24 during the campaign but have been estimated to be present at an upper limit constant  
25 concentration of 1 ppbV and which photolyse at a rate of ~3 × 10<sup>-5</sup> s<sup>-1</sup> at midday (Bejan et  
26 al., 2006).

27 f.) Photolysis of adsorbed HNO<sub>3</sub> on ground surfaces has been reported to produce HONO  
28 (Zhou et al., 2003; Zhou et al. 2011). We have estimated the concentration of HNO<sub>3</sub>  
29 deposited to the ground surface from the gas-phase HNO<sub>3</sub> concentration that was measured  
30 during ClearfLo and from the wind speed dependent  $\nu_{\text{HNO}_3}$  (Zhou et al., 2011). To assess

1 the maximum impact of this potential HONO source, a noon photolysis rate of surface  
2  $\text{HNO}_3$  of  $6 \times 10^{-5} \text{ s}^{-1}$ , two orders of magnitude faster than  $j(\text{HNO}_3)_g$  ( $j(\text{HNO}_3)_{0^\circ\text{SZA}} = 6 \times 10^{-7} \text{ s}^{-1}$ ) in the gas phase, has been taken (Zhou et al., 2011) and a 100 % HONO yield was  
3 assumed.  
4

5 g.) Photolysis of nitrate aerosols. To assess the maximum impact of this potential HONO  
6 source, a noon photolysis rate of aerosol  $\text{NO}_3^-$  of  $6 \times 10^{-5} \text{ s}^{-1}$  and a 100 % HONO yield was  
7 again assumed.

8 h.) Photosensitised heterogeneous conversion of  $\text{NO}_2$  to HONO on ground surfaces has been  
9 parameterised and included in the model by taking a ground surface conversion, which  
10 correlates with  $\text{NO}_2$  photolysis. A wind speed dependent  $\text{NO}_2$  deposition velocity  
11 calculated using  $1/R_c = 1 \text{ cm s}^{-1}$  (Joyce et al., 2014) in 75 m BL leads to a first order loss of  
12  $\text{NO}_2$  to the ground at a rate of  $4 \times 10^{-5} \text{ s}^{-1}$  on average, this is multiplied by a scaling factor  
13 equal to  $0.25 \times j(\text{NO}_2)$  which leads to an overall photosensitized conversion of  $\text{NO}_2 \rightarrow$   
14 HONO of  $\sim 5.6 \times 10^{-6} \text{ s}^{-1}$  during the day on average; consistent with the light induced  
15 conversion of  $\text{NO}_2$  to HONO observed in laboratory studies on humic acid surfaces  
16 (Stemmler et al 2007).

17 We do not include desorption of adsorbed HONO from soil (Oswald et al., 2013, 2015;  
18 VandenBoer et al., 2013) as they are still largely speculative, depend on many uncertain  
19 variables (soil pH, bacterial activity, soil humidity) and most probably have a very minor  
20 contribution under our highly urban conditions (low soil coverage, different expected diurnal  
21 contribution).

22

23

24 The full time series of the modelled HONO using the MCM, along with the measured values  
25 for the entire measurement campaign are shown in figure 4. Due to the difficulties of  
26 predicting nighttime chemistry with a photochemical model (such as the MCM), we only  
27 consider here the daytime (08:00 – 20:00). The time series show that predicted daytime  
28 HONO using the full model is higher than from the simple PSS calculation, however, it can  
29 be seen that the predicted daytime HONO is still lower than the measurement on all days and  
30 falls outside the 10% error of the LOPAP instrument. The average daytime diurnal cycle of  
31 the measured and modelled HONO, along with the contribution of the different sources in the

1 model is shown in figure 5. From just after sunrise (08:00), the contribution to HONO of the  
2 reaction between OH and NO decreases quickly due to the increasing  $j(\text{HONO})$  and  
3 decreasing NO levels throughout the morning. The largest contribution throughout the day  
4 comes from the photolysis of adsorbed  $\text{HNO}_3$ , contributing around 50% of the HONO source  
5 at midday. There are small contributions during the day and from heterogeneous conversion  
6 of  $\text{NO}_2$  (on both aerosol and ground surfaces) and the photolysis of ortho-nitro-phenol.  
7 Examining the total HONO predicted by the model compared to the measurement shows a  
8 significant underestimation of the modelled HONO compared to the measurement. They do  
9 both follow a similar diurnal cycle, with a decrease in HONO until around 16:00, followed by  
10 an increase into the evening, however the modelled HONO is up to a factor of around 2 lower  
11 than the measurement throughout the day. Subtracting the modelled from the measured  
12 HONO gives us a quantity that can be described as ‘missing’ HONO source, and average  
13 diurnal daytime profile of this is plotted in figure 6. The amount of the missing HONO source  
14 begins to increase at 08:00 and reaches a maximum at 12:00 of  $\sim 2.8 \text{ ppbV hr}^{-1}$ , exhibiting a  
15 similar diurnal trend to that of the HONO /  $\text{NO}_x$  ratio (see figure 2). It then starts to decrease  
16 throughout the afternoon and into the evening. Further analysis can be carried out by  
17 examining the diurnal profiles in the easterly and westerly flow conditions described earlier.  
18 Both conditions show broadly the same diurnal profile, however the daytime peak in missing  
19 HONO is greater in the more polluted easterly flow (up to 0.6 ppbV). This suggests that any  
20 missing source of HONO is related in some way to the pollution loading, most likely the  
21 amount of  $\text{NO}_2$ . This will be discussed further in later sections.

22 It is clear from this data, that neither a photostationary state calculation nor a more complete  
23 photochemical model containing currently known and postulated sources of HONO (that are  
24 relevant for this environment) can reproduce the daytime levels measured in London during  
25 this study. This is potentially significant, as HONO can be a large source of free radicals in  
26 such an urban environment, and any missing source in models can lead to an underestimation  
27 of the oxidising capacity of the atmosphere, and hence its ability to produce  $\text{O}_3$ . Therefore it is  
28 worth considering where the ‘missing’ HONO may come from and the importance of any  
29 extra source to the atmospheric oxidation capacity.

30

## 31 **4 Discussion**

### 32 **4.1 Instrument interference**

1 It is first worth considering the effect of possible instrument interferences on the HONO  
2 measurements made in this study. As described earlier, the LOPAP technique is not direct  
3 rather it measures HONO by conversion to a coloured azo dye which is then detected by  
4 absorption spectroscopy. However, it has been postulated that HO<sub>2</sub>NO<sub>2</sub> could interfere with  
5 the conversion reaction, leading to erroneous HONO measurements. A recent study by  
6 (Legrand et al., 2014), using an identical instrument to the one described here and  
7 investigating apparently high measurements of HONO in Antarctica, showed in laboratory  
8 experiments that the instrument does have an interference with HO<sub>2</sub>NO<sub>2</sub>. Their work  
9 indicated that up to 15% of HO<sub>2</sub>NO<sub>2</sub> was converted to the azo dye in the instrument and  
10 detected as HONO. For this study, 2 ppbv of HO<sub>2</sub>NO<sub>2</sub> would explain the difference between  
11 measured and modelled HONO, however this seems unrealistic in an urban environment in  
12 summer (Dentener et al., 2002). In fact, the box model used here shows HO<sub>2</sub>NO<sub>2</sub> levels to  
13 only be between 2 – 10 pptv, therefore we feel that this instrument interference can be  
14 discounted here. For submicrometer particles we exclude any interferences by particle nitrite,  
15 since their sampling efficiency is <2 % in the very short stripping coil (4 coil sampler). Even  
16 if that increased to values of 10 % for larger coarse particles, such interference would be  
17 almost perfectly corrected for by the two channel approach. For much larger fog particles  
18 (which actually were not present during the campaign during daytime) interferences would be  
19 only expected in the case of high fog pH values of >5. For lower pH, expected for the urban  
20 conditions in London, the effective solubility of HONO (HONO + nitrite) would be too low to  
21 significantly influence the HONO data, even for high uptake efficiency of fog particles.  
22 Accordingly, we do not consider particle interferences as an important issue. Finally, the  
23 LOPAP was successfully inter-compared to the spectroscopic DOAS technique under urban  
24 background conditions similar to the present study (Kleffmann et al., 2006).

25

## 26 **4.2 Missing HONO source**

27 The ClearfLo IOP campaign involved a wide range of measurements, thus enabling the  
28 relationship between the apparent missing HONO and various other species to be  
29 investigated. Initially, daytime diurnal average profiles were plotted for NO<sub>2</sub> and the product  
30 NO<sub>2</sub> × *j*(NO<sub>2</sub>), along with the extra rate of production of HONO required for the model to  
31 reproduce the measurements (termed ‘missing HONO source’ - figure 7). The plots show that,  
32 whilst there is little correlation between the NO<sub>2</sub> on its own with the missing HONO, there

1 appears to be a reasonable correlation with the product of  $\text{NO}_2$  and  $j(\text{NO}_2)$ , hence pointing  
2 towards a photolytic source.

3 To further investigate any potential correlation, the full data series of the missing HONO  
4 source and different input data are normalised to 1 and correlated against each other. The  
5 normalised missing HONO source data are then correlated with the normalised products of all  
6 possible combinations of the input data. The datasets are then filtered to determine if  
7 inclusion of an extra dataset has led to a genuine increase in the correlation coefficient. For  
8 inclusion in the filtered output, the correlation coefficient for the product must be greater than  
9 the correlation coefficient for each of the individual components in the product. Additionally,  
10 inclusion of an additional dataset in a product must lead to an increase in the correlation  
11 coefficient for the new product when compared to the correlation coefficient without that new  
12 dataset. Datasets included are:  $j(\text{NO}_2)$  (used as a proxy for radiation), water vapour,  $\text{NO}$ ,  $\text{NO}_2$ ,  
13 temperature, adsorbed  $\text{HNO}_3$  ( $\text{HNO}_3_{\text{ads.}}$ ),  $\text{OH}$ ,  $\text{HO}_2$ ,  $\text{RO}_2$ ,  $\text{OH}$  reactivity ( $k(\text{OH})$ ), nitrate  
14 aerosol ( $\text{NO}_3^-_{\text{aero.}}$ ), ammonium aerosol ( $\text{NH}_4^+_{\text{aero.}}$ ) and aerosol surface area (SA). We use  
15  $k(\text{OH})$  as a proxy for organic substances as it has been shown by Whalley et al., 2015b, that  
16  $k(\text{OH})$  is largely controlled by VOCs during the measurement period (typically 80% during  
17 daytime). The correlation plots are shown in the supplementary information (figure S1), with  
18 the correlation coefficients of the different combinations presented in table 1. The data shows  
19 that several product combinations are significantly higher than those of the individual  
20 components. For instance, the correlation coefficient with  $\text{NO}_2$  alone is virtually zero,  
21 whereas for the product of  $j(\text{NO}_2) \times \text{NO}_2$  the  $r^2$  is 0.696, for  $j(\text{NO}_2) \times k(\text{OH})$  it is 0.678 and for  
22  $\text{NO}_2 \times k(\text{OH}) \times j(\text{NO}_2)$  the  $r^2$  is 0.659. Thus, if gaseous VOCs (represented here by  $k(\text{OH})$ ) are  
23 precursors for VOCs adsorbed onto surfaces, then this is an indication that the photosensitised  
24 reaction of  $\text{NO}_2$  on surfaces containing organics as a source of HONO may currently be  
25 under-estimated in the model. We also see high correlation coefficients with  $j(\text{NO}_2) \times T$   
26 (0.628), however this can be explained by radiation and temperature following a similar  
27 diurnal pattern, albeit with a slight (1 - 2 hours) time lag. The product of  $j(\text{NO}_2)$  and  
28 ammonium aerosol ( $\text{NH}_4^+$ ) is 0.583, suggesting this may play a role in the missing HONO,  
29 although any possible mechanisms for this are unclear.

30 In order to investigate the day-to-day variation in the potential HONO source, correlation  
31 plots were made of the daytime average (08:00 – 20:00) missing HONO source against  $\text{NO}_2$   
32 and the product of  $j(\text{NO}_2)$  with  $\text{NO}_2$ ,  $k(\text{OH})$  and  $\text{NO}_2 \times k(\text{OH})$  (figure 8). These show that

1 there is some correlation for all species, with the products of the species with  $j(\text{NO}_2)$  ( $r^2 =$   
2 0.64, 0.55 and 0.71 for  $\text{NO}_2$ ,  $k(\text{OH})$  and  $\text{NO}_2 \times k(\text{OH})$  respectively) being significantly higher  
3 than with  $\text{NO}_2$  alone ( $r^2$  0.33).

4 Based on the correlational analysis we propose here an enhancement in the photosensitized  
5 conversion of  $\text{NO}_2$  on organic substrates to explain the missing HONO source. In contrast,  
6 other recently proposed HONO sources will have a minor contribution. Aqueous solutions in  
7 which HONO yields from nitrate photolysis may be enhanced by organics (Scharko et al.,  
8 2014) will be not important for the urban conditions investigated in this study as there are no  
9 aqueous surfaces in the surrounding area. Or recently, in the study of Rutter et al. (2014), a  
10 gas phase reduction of  $\text{HNO}_3$  by VOCs to HONO was proposed. However, since the  
11 conditions of that laboratory study were not atmospherically relevant (reaction in the presence  
12 of ca. 200 ppb of a high molecular weight motor oil), we have not considered this source for  
13 this analysis. In addition, this is a dark reaction, while we have mainly considered the more  
14 important daytime HONO chemistry in the present manuscript. In the study of Ziemba et al.  
15 (2010) a conversion of  $\text{HNO}_3$  on organic aerosols was proposed based on field observations.  
16 However, HONO formation was only observed in the dark, which again is out of the scope of  
17 this study. In addition the very low correlation coefficient of the missing HONO source with  
18 aerosol nitrate does not support this mechanism. Formation of HONO by soil sources (Oswald  
19 et al., 2013, 2015) are also expected to be of minor importance for London, due to low soil  
20 surface coverage.

21 Although direct emissions were already considered in the model, we carried out a sensitivity  
22 analysis into the direct emission of HONO, to study potential errors within our model. We  
23 found that increasing direct emissions by a factor of 2 (even though we think our estimate is  
24 already an upper limit), only results in a 4% increase in the modelled HONO. Hence we do  
25 not believe direct emissions to be the source of the missing HONO. We have also run a  
26 sensitivity analysis on the heterogeneous photosensitized conversion of  $\text{NO}_2$  on ground  
27 surfaces by increasing the conversion rate by up to a factor of 10 to assess the impact of  
28 enhanced reactive uptake of  $\text{NO}_2$  on other surfaces, for example urban grime. We find that a  
29 reactive conversion rate of  $\sim 6 \times 10^{-5} \text{ s}^{-1}$  (but which varies as a function of  $j(\text{NO}_2)$ ) closes the  
30 daytime HONO budget at all times (apart from the late afternoon). This is shown in figure 9,  
31 demonstrating that with an increased conversion rate, the heterogeneous photosensitized  
32 conversion of  $\text{NO}_2$  on ground surfaces becomes the largest HONO source throughout the day.

1 Based on this sensitivity study and on the high correlation of the missing HONO source with  
2 the product  $j(\text{NO}_2) \times \text{NO}_2$  and  $j(\text{NO}_2) \times \text{NO}_2 \times k(\text{OH})$  enhanced photosensitized conversion of  
3  $\text{NO}_2$  on organic surfaces is proposed here as a major HONO source in London. However, the  
4 exact identification of the organics adsorbed on the urban surfaces (humic acids, organic  
5 grime, etc.) is out of the scope of the present study. In Sörgel et al. 2011b, it was shown that  
6 the results presented by Stemmler et al., 2007 on an artificial humic acid are not able to  
7 describe their field observation. The heterogeneous  $\text{NO}_2$  uptake kinetics and HONO yields of  
8 real urban organic substrates are not known and maybe different compared to the artificial  
9 surfaces studied in the laboratory. Detailed laboratory studies on real surfaces collected from  
10 the surrounding of the field site in London would be necessary, which is again out of the  
11 scope of this study.

12 It should also be pointed out that our model only represents the situation at the measurement  
13 height of HONO and the supporting species (5 m) and is not used to attempt to describe the  
14 entire boundary layer. Numerous measurements demonstrate that near-surface vertical  
15 structure in HONO can be significant at night and during the day (Stutz et al., 2002;  
16 Kleffmann, 2003; 2007; Zhang et al., 2009; Villena et al., 2011; Wong et al., 2012; Young et  
17 al., 2012; Oswald et al., 2015) and that a model using a near-surface source distributed  
18 throughout the boundary layer produces results inconsistent with observations (Vandenboer et  
19 al., 2013; Wong et al., 2013; Kim et al., 2014; Sörgel et al., 2015). Thus, some of the  
20 discrepancy between the model and measurements, particularly in the early morning when  
21 thermal inversions can persist, could be ascribed to biases from vertical stratification in  
22 HONO. It is, however, clear that at the present urban background site close to central London  
23 and within 5 meters of the surface, a significant missing source of HONO is active when  
24 compared to the output of a box model containing most known sources. We suggest from our  
25 analysis of the supporting data that processes responsible for the unknown source of HONO  
26 in this particular study are at least partially connected with light,  $\text{NO}_2$  and organic matter  
27 (represented by  $k(\text{OH})$ ), in agreement with the source described in Stemmler et al. (2006;  
28 2007).

29

### 1 **4.3 HONO contribution to atmospheric oxidation**

2 HONO is known to be an important initiation source of OH radicals (Ren et al., 2003; Ren et  
3 al., 2006; Dusanter et al., 2009; Elshorbany et al., 2009; Hofzumahaus et al., 2009; Villena et  
4 al., 2011; Michoud et al., 2012; Michoud et al., 2014), so any extra source that is not well  
5 understood or defined in models could have a potentially important impact on atmospheric  
6 oxidation capacity and hence O<sub>3</sub> and secondary organic aerosol (SOA) production. The model  
7 described above was used to produce a rate of production analysis (ROPA) for OH radicals  
8 during the measurements campaign, with a view to assessing the importance of HONO and in  
9 particular the missing HONO source. It should again be pointed out here that any conclusions  
10 drawn from this analysis are only valid for this particular measurement site (i.e. close to the  
11 surface). The model is only being used to understand OH production at the HONO  
12 measurement height even though the chemistry is taking place in a dynamic boundary layer.  
13 For the analysis of the vertical structure of the HONO contribution to the OH initiation, our  
14 measurement data is not sufficient and further gradient studies would be necessary. We also  
15 do not include the enhanced reactive conversion of NO<sub>2</sub> on other surfaces nor increased direct  
16 emissions described in the sensitivity analysis in this investigation.

17 For this analysis, the ROPA output was plotted for all OH radical sources and the diurnal  
18 average for these is shown in figure 10. Initially ignoring the missing HONO source, it can be  
19 seen that in the early morning shortly after sunrise, HONO is a significant OH source (30 –  
20 40% of the total, second only to the propagation source of NO + HO<sub>2</sub>). This is due to the  
21 build-up of HONO concentrations overnight, followed by its rapid photolysis after sunrise.  
22 Then, approaching solar noon, whilst the absolute production rate from HONO photolysis  
23 remains relatively constant, the dominant OH source becomes the HO<sub>2</sub> + NO reaction. At  
24 solar noon, HONO unconstrained in the model accounts for around 40% of the total OH  
25 radical sources and 57% of the HO<sub>x</sub> initiation sources. During the late afternoon and evening  
26 approaching sunset, OH from HONO photolysis again becomes comparable to HO<sub>2</sub> + NO.  
27 The photolysis of O<sub>3</sub> is only a minor component of the total OH radical sources throughout  
28 the day, peaking at around 10% in early afternoon. The same holds for the ozonolysis of  
29 alkenes which is caused, at least in part, by the low levels of measured alkenes. With the  
30 model constrained to the measured HONO, it was possible to add on the effect of the missing  
31 HONO source to OH radical production rate to the diurnal profile. It can clearly be seen that  
32 the OH production rate is significantly increased during the daytime, especially during the

1 afternoon when constraining the model to measured HONO, where the OH production rate  
2 increases by around 20%. This result shows that, even when all currently known sources of  
3 HONO are added to a box model, missing HONO sources are still crucial to HO<sub>x</sub> radical  
4 production at the surface, which is directly relevant to atmospheric oxidation capacity and O<sub>3</sub>  
5 formation.

6 This importance is also shown when the model is used to calculate OH concentrations, as  
7 shown in figure 11. If the model is run with PSS calculated HONO (i.e. only OH + NO as a  
8 source), there is a significant under prediction of OH levels (~40% during daytime). When the  
9 known or postulated HONO sources are included in the model, the predicted OH is increased  
10 by a factor of 1.4 – 1.6 during the day. However, during the afternoon, predicted OH is still  
11 20 – 30% lower than modelled, suggesting a missing OH source. It is only when the model is  
12 constrained to measured HONO the agreement between measured and modelled OH becomes  
13 good (<5% discrepancy at midday and during most of the afternoon) and within the  
14 experimental error of the measurements (~15%). This clearly demonstrates the need for  
15 models to include accurate HONO data (either from measurements or a model containing all  
16 HONO sources and sinks) and thus shows the need for further investigation on the missing  
17 HONO source to be carried out.

## 18 **5 Summary and Conclusions**

19 In this study a month long time series of HONO levels at an urban background site in London  
20 was measured, with average mixing ratios showing a peak in the early morning of ~0.6 ppbV  
21 and a minimum during early afternoon of ~0.18 ppbV. Analysis of the HONO / NO<sub>x</sub> ratio  
22 showed a significant secondary peak during daytime, suggesting additional sources of HONO  
23 other than the reaction between NO and OH. The presence of a large range of other  
24 atmospheric gas and aerosol measurements (including OH and HO<sub>2</sub> radicals), allowed a  
25 detailed study of known and postulated production routes of HONO to be undertaken, using  
26 both a simple PSS analysis and a box model based on the MCMv3.2. The calculated HONO  
27 shows a daytime underestimation of ~0.2 ppbV on average, even when recently suggested  
28 sources such as the reaction of HO<sub>2</sub>×H<sub>2</sub>O with NO<sub>2</sub> to produce HONO, photolysis of adsorbed  
29 HNO<sub>3</sub>, photo-enhanced conversion of NO<sub>2</sub> on ground and aerosol surfaces and direct traffic  
30 emissions are included, again suggesting a significant missing HONO source. Correlation  
31 plots of the missing HONO production rate against various other species measured at the site  
32 show a reasonable correlation with the product of  $j(NO_2)$  with NO<sub>2</sub> and  $k(OH)$ , suggesting

1 that the proposed photosensitized heterogeneous conversion of  $\text{NO}_2$  to HONO on organic  
2 substrates as observed in laboratory studies may be enhanced under these urban conditions.

3 The effect of the missing source of HONO to the oxidising capacity of the urban background  
4 atmosphere has been investigated using radical rate of production analyses. These show that  
5 OH radical production during the day increases by over 20% if measured HONO is used in  
6 the model as compared to allowing the model to run unconstrained to HONO, even with  
7 known and postulated HONO sources included. In addition, modelled OH only reproduces the  
8 measurement when HONO was constrained in the model. Whilst our results are only valid at  
9 the surface due to the likely HONO gradients, it is still an important result and demonstrates  
10 the need of a full understanding of the HONO production processes in an urban area such as  
11 London in, for example, air quality prediction models. The results presented here provide  
12 further evidence that unknown sources of HONO are present in the urban environment, and  
13 they are probably a function of  $\text{NO}_x$  and sunlight. It is not possible to conclude exactly the  
14 origin of the source from this work, hence further field measurements and, probably more  
15 crucially, laboratory studies are needed to investigate these important processes further.

16

## 17 **Acknowledgements**

18 The authors would like to thank the staff and governors of The Sion Manning RC School,  
19 North Kensington, London for hosting the field campaign. Thanks also go to Brian Bandy  
20 from the University of East Anglia for HCHO and Janet Barlow and Christoforos Halios from  
21 the University of Reading for boundary layer height data. The work was funded through the  
22 UK Natural Environment Research Council (NERC) ClearfLo project (grant number  
23 NE/H003223/1).

## 1 **References**

- 2 Acker, K., Möller, D., Wieprecht, W., Meixner, F. X., Bohn, B., Gilge, S., Plass-Dülmer, C.,  
3 and Berresheim, H.: Strong daytime production of OH from HNO<sub>2</sub> at a rural mountain site,  
4 *Geophys. Res. Lett.*, 33, L02809, 10.1029/2005gl024643, 2006.
- 5 Alicke, B., Platt, U., and Stutz, J.: Impact of nitrous acid photolysis on the total hydroxyl  
6 radical budget during the Limitation of Oxidant Production/Pianura Padana Produzione di  
7 Ozono study in Milan, *J. Geophys. Res.*, 107, 8196, 10.1029/2000jd000075, 2002.
- 8 Arens, F., L. Gutzwiller, U. Baltensperger, H. W. Gäggeler, and M. Ammann: Heterogeneous  
9 Reaction of NO<sub>2</sub> on Diesel Soot Particles, *Environ. Sci. Technol.*, 35, 2191-2199, 2001.
- 10 Atkinson, R., Baulch, D. L., Cox, R. A., Crowley, J. N., Hampson, R. F., Hynes, R. G.,  
11 Jenkin, M. E., Rossi, M. J., and Troe, J.: Evaluated kinetic and photochemical data for  
12 atmospheric chemistry: Volume I - gas phase reactions of O<sub>x</sub>, HO<sub>x</sub>, NO<sub>x</sub> and SO<sub>x</sub> species,  
13 *Atmos. Chem. Phys.*, 4, 1461-1738, 10.5194/acp-4-1461-2004, 2004.
- 14 Barlow, J. F., Dunbar, T. M., Nemitz, E. G., Wood, C. R., Gallagher, M. W., Davies, F.,  
15 O'Connor, E., and Harrison, R. M.: Boundary layer dynamics over London, UK, as observed  
16 using Doppler lidar during REPARTEE-II, *Atmos. Chem. Phys.*, 11, 2111-2125, 10.5194/acp-  
17 11-2111-2011, 2011.
- 18 Barlow, J. F., Halios, C. H., Lane, S. E., and Wood, C. R.: Observations of urban boundary  
19 layer structure during a strong urban heat island event, *Environ. Fluid Mech.*, 15(2), 373-398,  
20 10.1007/s10652-014-9335-6, 2015.
- 21 Bejan, I., Abd El Aal, Y., Barnes, I., Benter, T., Bohn, B., Wiesen, P., and Kleffmann, J.: The  
22 photolysis of ortho-nitrophenols: a new gas phase source of HONO, *Phys. Chem. Chem.*  
23 *Phys.*, 8, 2028-2035, 10.1039/b516590c, 2006.
- 24 Bigi, A., and Harrison, R. M.: Analysis of the air pollution climate at a central urban  
25 background site, *Atmos. Environ.*, 44, 2004-2012, 10.1016/j.atmosenv.2010.02.028, 2010.
- 26 Bohnenstengel, S. I., Belcher, S. E., Aiken, A., Allan, J. D., Allen, G., Bacak, A., Bannan, T.  
27 J., Barlow, J. F., Beddows, D. C. S., Bloss, W. J., Booth, A. M., Chemel, C., Coceal, O., Di  
28 Marco, C. F., Dubey, M. K., Faloon, K. H., Fleming, Z. L., Furger, M., Gietl, J. K., Graves,  
29 R. R., Green, D. C., Grimmond, C. S. B., Halios, C. H., Hamilton, J. F., Harrison, R. M.,  
30 Heal, M. R., Heard, D. E., Helfter, C., Herndon, S. C., Holmes, R. E., Hopkins, J. R., Jones,

1 A. M., Kelly, F. J., Kotthaus, S., Langford, B., Lee, J. D., Leigh, R. J., Lewis, A. C., Lidster,  
2 R. T., Lopez-Hilfiker, F. D., McQuaid, J. B., Mohr, C., Monks, P. S., Nemitz, E., Ng, N. L.,  
3 Percival, C. J., Prévôt, A. S. H., Ricketts, H. M. A., Sokhi, R., Stone, D., Thornton, J. A.,  
4 Tremper, A. H., Valach, A. C., Visser, S., Whalley, L. K., Williams, L. R., Xu, L., Young, D.  
5 E., and Zotter, P.: Meteorology, air quality, and health in London: The ClearfLo project, B.  
6 Am. Meteorol. Soc., online, 10.1175/BAMS-D-12-00245.1, 2014.

7 Bush, T. J., Tsagatakis, I., King, K., and Passant, N. R.: NAEI UK Emission Mapping  
8 Methodology 2006, AEATY/ENV/R/2696, available at: <http://www.naei.org.uk/reoprts.php>,  
9 2006.

10 Cappa, C. D., Onasch, T. B., Massoli, P., Worsnop, D. R., Bates, T. S., Cross, E. S.,  
11 Davidovits, P., Hakala, J., Hayden, K. L., Jobson, B. T., Kolesar, K. R., Lack, D. A., Lerner,  
12 B. M., Li, S.-M., Mellon, D., Nuaaman, I., Olfert, J. S., Petäjä, T., Quinn, P. K., Song, C.,  
13 Subramanian, R., Williams, E. J., and Zaveri, R. A.: Radiative Absorption Enhancements Due  
14 to the Mixing State of Atmospheric Black Carbon, *Science*, 337, 1078-1081,  
15 10.1126/science.1223447, 2012.

16 Creasey, D. J., Heard, D. E., and Lee, J. D.: Absorption cross-section measurements of water  
17 vapour and oxygen at 185 nm. Implications for the calibration of field instruments to measure  
18 OH, HO<sub>2</sub> and RO<sub>2</sub> radicals, *Geophys. Res. Lett.*, 27, 1651-1654, 10.1029/1999gl011014,  
19 2000.

20 Dentener, F., Williams, J., and Metzger, S.: Aqueous phase reaction of HNO<sub>4</sub>: The impact on  
21 tropospheric chemistry, *J. Atmos. Chem.*, 41, 109-134, 10.1023/a:1014233910126, 2002.

22 Dransfield, T. J., Donahue, N. M., and Anderson, J. G.: High-Pressure Flow Reactor Product  
23 Study of the Reactions of HO<sub>x</sub> + NO<sub>2</sub>: The Role of Vibrationally Excited Intermediates†, *J.*  
24 *Phys. Chem. A*, 105, 1507-1514, 10.1021/jp002391+, 2001.

25 Drummond, J. W., Volz, A., and Ehhalt, D. H.: An Optimized Chemiluminescence Detector  
26 for Tropospheric NO Measurements, *J. Atmos. Chem.*, 2, 287-306, 10.1007/bf00051078,  
27 1985.

28 Dusanter, S., Vimal, D., Stevens, P. S., Volkamer, R., Molina, L. T., Baker, A., Meinardi, S.,  
29 Blake, D., Sheehy, P., Merten, A., Zhang, R., Zheng, J., Fortner, E. C., Junkermann, W.,  
30 Dubey, M., Rahn, T., Eichinger, B., Lewandowski, P., Prueger, J., and Holder, H.:

1 Measurements of OH and HO<sub>2</sub> concentrations during the MCMA-2006 field campaign - Part  
2 2: Model comparison and radical budget, *Atmos. Chem. Phys.*, 9, 6655-6675, 2009.

3 Edwards, G. D., and Monks, P. S.: Performance of a single-monochromator diode array  
4 spectroradiometer for the determination of actinic flux and atmospheric photolysis  
5 frequencies, *J. Geophys. Res.*, 108, 2003.

6 Elshorbany, Y. F., Kurtenbach, R., Wiesen, P., Lissi, E., Rubio, M., Villena, G., Gramsch, E.,  
7 Rickard, A. R., Pilling, M. J., and Kleffmann, J.: Oxidation capacity of the city air of  
8 Santiago, Chile, *Atmos. Chem. Phys.*, 9, 2257-2273, 2009.

9 Forster, G. L., Sturges, W. T., Fleming, Z. L., Bandy, B. J., and Emeis, S.: A year of H<sub>2</sub>  
10 measurements at Weybourne Atmospheric Observatory, UK, 2012, *Tellus B*, 64, 17771,  
11 10.3402/tellusb.v64i0.17771, 2012.

12 George, C., Strekowski, R. S., Kleffmann, J., Stemmler, K., and Ammann, M.:  
13 Photoenhanced uptake of gaseous NO<sub>2</sub> on solid organic compounds: a photochemical source  
14 of HONO?, *Faraday Discuss.*, 130, 195-210, 10.1039/b417888m, 2005.

15 Harrison, R. M. and Kitto, A.-M. N.: Evidence for a Surface Source of Atmospheric Nitrous  
16 Acid, *Atmos. Environ.*, 28, 1089-1094, 1994.

17 Heland, J., Kleffmann, J., Kurtenbach, R., and Wiesen, P.: A New Instrument To Measure  
18 Gaseous Nitrous Acid (HONO) in the Atmosphere, *Environ. Sci. Technol.*, 35, 3207-3212,  
19 10.1021/es000303t, 2001.

20 Hofzumahaus, A., Rohrer, F., Lu, K. D., Bohn, B., Brauers, T., Chang, C. C., Fuchs, H.,  
21 Holland, F., Kita, K., Kondo, Y., Li, X., Lou, S., Shao, M., Zeng, L., Wahner, A., and Zhang,  
22 Y.: Amplified Trace Gas Removal in the Troposphere, *Science*, 324, 1702-1704, 2009.

23 Hofzumahaus, A: Oral presentation during the conference: Atmospheric Chemical  
24 Mechanisms “Simple Models – Real World Complexities” December, 10-12, 2014, UC  
25 Davis.

26 Hopkins, J. R., Lewis, A. C., and Read, K. A.: A two-column method for long-term  
27 monitoring of non-methane hydrocarbons (NMHCs) and oxygenated volatile organic  
28 compounds (o-VOCs), *J. Environ. Monit.*, 5, 8-13, 2003.

29 Jenkin, M. E., Wyche, K. P., Evans, C. J., Carr, T., Monks, P. S., Alfarra, M. R., Barley, M.  
30 H., McFiggans, G. B., Young, J. C., and Rickard, A. R.: Development and chamber

1 evaluation of the MCM v3.2 degradation scheme for beta-caryophyllene, *Atmos. Chem.*  
2 *Phys.*, 12, 5275-5308, 10.5194/acp-12-5275-2012, 2012.

3 Joyce, P. L., von Glasow, R., and Simpson, W. R.: The fate of NO<sub>x</sub> emissions due to  
4 nocturnal oxidation at high latitudes: 1-D simulations and sensitivity experiments, *Atmos.*  
5 *Chem. Phys.*, 14, 7601-7616, 10.5194/acp-14-7601-2014, 2014.

6 Kim, S., Vandenboer, T. C., Young, C. J., Riedel, T. P., Thornton, J. A., Swarthout, B., Sive,  
7 B., Lerner, B., Gilman, J. B., Warneke, C., Roberts, J. M., Guenther, A. B., Wagner, N. L.,  
8 Dubé, W. P., Williams, E. and Brown, S. S.: The primary and recycling sources of OH during  
9 the NACHT-2011 campaign: HONO as an important OH primary source in the wintertime, *J.*  
10 *Geophys. Res.*, 119, 6886–6896, doi:10.1002/2013JD020225, 2014.

11 Kleffmann, J., K. H. Becker, M. Lackhoff, and P. Wiesen: Heterogeneous Conversion of NO<sub>2</sub>  
12 on Carbonaceous Surfaces, *Phys. Chem. Chem. Phys.*, 1, 5443-5450, 1999.

13 Kleffmann, J., R. Kurtenbach, J. Lörzer, P. Wiesen, N. Kalthoff, B. Vogel, and H. Vogel:  
14 Measured and Simulated Vertical Profiles of Nitrous Acid, Part I: Field Measurements,  
15 *Atmos. Environ.*, 37, 2949-2955, 2003.

16 Kleffmann, J., Gavrioloaiei, T., Hofzumahaus, A., Holland, F., Koppmann, R., Rupp, L.,  
17 Schlosser, E., Siese, M., and Wahner, A.: Daytime formation of nitrous acid: A major source  
18 of OH radicals in a forest, *Geophys. Res. Lett.*, 32, L05818, 10.1029/2005gl022524, 2005.

19 Kleffmann, J., Lörzer, J. C., Wiesen, P., Kern, C., Trick, S., Volkamer, R., Rodenas, M., and  
20 Wirtz, K.: Intercomparison of the DOAS and LOPAP techniques for the detection of nitrous  
21 acid (HONO), *Atmos. Environ.*, 40, 3640-3652, 10.1016/j.atmosenv.2006.03.027, 2006.

22 Kleffmann, J.: Daytime sources of nitrous acid (HONO) in the atmospheric boundary layer,  
23 *Chem. Phys. Chem.*, 8, 1137-1144, 10.1002/cphc.200700016, 2007.

24 Kraus, A., and Hofzumahaus, A.: Field measurements of atmospheric photolysis frequencies  
25 for O<sub>3</sub>, NO<sub>2</sub>, HCHO, CH<sub>3</sub>CHO, H<sub>2</sub>O<sub>2</sub>, and HONO by UV spectroradiometry, *J. Atmos.*  
26 *Chem.*, 31, 161-180, 10.1023/a:1005888220949, 1998.

27 Kurtenbach, R., Becker, K. H., Gomes, J. A. G., Kleffmann, J., Lörzer, J. C., Spittler, M.,  
28 Wiesen, P., Ackermann, R., Geyer, A., and Platt, U.: Investigations of emissions and  
29 heterogeneous formation of HONO in a road traffic tunnel, *Atmos. Environ.*, 35, 3385-3394,  
30 10.1016/s1352-2310(01)00138-8, 2001.

1 Lee, J. D., Moller, S. J., Read, K. A., Lewis, A. C., Mendes, L., and Carpenter, L. J.: Year-  
2 round measurements of nitrogen oxides and ozone in the tropical North Atlantic marine  
3 boundary layer, *J. Geophys. Res.*, 114, D21302, 10.1029/2009jd011878, 2009.

4 Lee, B. H., Wood, E. C., Herndon, S. C., Lefer, B. L., Luke, W. T., Brune, W. H., Nelson, D.  
5 D., Zahniser, M. S., and Munger, J. W.: Urban measurements of atmospheric nitrous acid: A  
6 caveat on the interpretation of the HONO photostationary state, *J. Geophys. Res. Atmos.*, 118,  
7 10.1002/2013JD020341, 2013.

8 Legrand, M., Preunkert, S., Frey, M., Bartels-Rausch, T., Kukui, A., King, M. D., Savarino,  
9 J., Kerbrat, M., and Jourdain, B.: Large mixing ratios of atmospheric nitrous acid (HONO) at  
10 Concordia (East Antarctic Plateau) in summer: a strong source from surface snow?, *Atmos.*  
11 *Chem. Phys.*, 14, 9963-9976, 10.5194/acp-14-9963-2014, 2014.

12 Levy II, H.: Normal Atmosphere: Large Radical and Formaldehyde Concentrations Predicted,  
13 *Science*, 173, 141-143, 1971.

14 Li, S., Matthews, J., and Sinha, A.: Atmospheric hydroxyl radical production from  
15 electronically excited NO<sub>2</sub> and H<sub>2</sub>O, *Science*, 319, 1657-1660, 10.1126/science.1151443,  
16 2008.

17 Li, X., Rohrer, F., Hofzumahaus, A., Brauers, T., Häsel, R., Bohn, B., Broch, S., Fuchs, H.,  
18 Gomm, S., Holland, F., Jäger, J., Kaiser, J., Keutsch, F. N., Lohse, I., Lu, K., Tillmann, R.,  
19 Wegener, R., Wolfe, G. M., Mentel, T. F., Kiendler-Scharr, A., and Wahner, A.: Missing Gas-  
20 Phase Source of HONO Inferred from Zeppelin Measurements in the Troposphere, *Science*,  
21 344, 292-296, 10.1126/science.1248999, 2014.

22 Lidster, R. T., Hamilton, J. F., Lee, J. D., Lewis, A. C., Hopkins, J. R., Punjabi, S., Rickard,  
23 A. R., and Young, J. C.: The impact of monoaromatic hydrocarbons on OH reactivity in the  
24 coastal UK boundary layer and free troposphere, *Atmos. Chem. Phys.*, 14, 6677-6693,  
25 10.5194/acp-14-6677-2014, 2014.

26 Michoud, V., Kukui, A., Camredon, M., Colomb, A., Borbon, A., Miet, K., Aumont, B.,  
27 Beekmann, M., Durand-Jolibois, R., Perrier, S., Zapf, P., Siour, G., Ait-Helal, W., Locoge,  
28 N., Sauvage, S., Afif, C., Gros, V., Furger, M., Ancellet, G., and Doussin, J. F.: Radical  
29 budget analysis in a suburban European site during the MEGAPOLI summer field campaign,  
30 *Atmos. Chem. Phys.*, 12, 11951-11974, 10.5194/acp-12-11951-2012, 2012.

1 Michoud, V., Colomb, A., Borbon, A., Miet, K., Beekmann, M., Camredon, M., Aumont, B.,  
2 Perrier, S., Zapf, P., Siour, G., Ait-Helal, W., Afif, C., Kukui, A., Furger, M., Dupont, J. C.,  
3 Haeffelin, M., and Doussin, J. F.: Study of the unknown HONO daytime source at a European  
4 suburban site during the MEGAPOLI summer and winter field campaigns, *Atmos. Chem.*  
5 *Phys.*, 14, 2805-2822, 10.5194/acp-14-2805-2014, 2014.

6 Monge, M. E., D'Anna, B., Mazri, L., Giroir-Fendler, A., Ammann, M., Donaldson, D. J., and  
7 George, C.: Light changes the atmospheric reactivity of soot, *Proc. Natl. Acad. Sci. U.S.A.*,  
8 107, 6605-6609, 10.1073/pnas.0908341107, 2010.

9 Oswald R., Behrendt, T., Ermel, M., Wu, D., Su, H., Cheng, Y., Breuninger, C., Moravek, A.,  
10 Mougín, E., Delon, C., Loubet, B., Pommerening-Röser, A., Sörgel, M., Pöschl, U.,  
11 Hoffmann, T., Andreae, M. O., Meixner, F. X., and Trebs, I.: HONO Emissions from Soil  
12 Bacteria as a Major Source of Atmospheric Reactive Nitrogen, *Science*, 341, 1233-1235,  
13 2013.

14 Oswald, R., Ermel, M., Hens, K., Novelli, A., Ouwersloot, H. G., Paasonen, P., Petäjä, T.,  
15 Sipilä, M., Kerónen, P., Bäck, J., Königstedt, R., Hosaynali Beygi, Z., Fischer, H., Bohn, B.,  
16 Kubistin, D., Harder, H., Martinez, M., Williams, J., Hoffmann, T., Trebs, I. and Sörgel, M.:  
17 Comparison of HONO budgets for two measurement heights at a field station within the  
18 boreal forest in Finland, *Atmos. Chem. Phys.*, 15, 799–813, doi:10.5194/acp-15-799-2015,  
19 2015.

20 Pollack, I. B., Lerner, B. M., and Ryerson, T. B.: Evaluation of ultraviolet light-emitting  
21 diodes for detection of atmospheric NO<sub>2</sub> by photolysis - chemiluminescence, *J. Atmos.*  
22 *Chem.*, 65, 111-125, 10.1007/s10874-011-9184-3, 2010.

23 Qin, M., Xie, P., Su, H., Gu, J., Peng, F., Li, S., Zeng, L., Liu, J., Liu, W., and Zhang, Y.: An  
24 observational study of the HONO-NO<sub>2</sub> coupling at an urban site in Guangzhou City, South  
25 China, *Atmos. Environ.*, 43, 5731-5742, 10.1016/j.atmosenv.2009.08.017, 2009.

26 Ren, X. R., Harder, H., Martinez, M., Leshner, R. L., Oliger, A., Simpas, J. B., Brune, W. H.,  
27 Schwab, J. J., Demerjian, K. L., He, Y., Zhou, X., and Gao, H.: OH and HO<sub>2</sub> chemistry in the  
28 urban atmosphere of New York City, *Atmos. Environ.*, 37, 3639-3651, 2003.

29 Ren, X., Brune, W. H., Oliger, A., Metcalf, A. R., Simpas, J. B., Shirley, T., Schwab, J. J.,  
30 Bai, C. H., Roychowdhury, U., Li, Y. Q., Cai, C. X., Demerjian, K. L., He, Y., Zhou, X. L.,  
31 Gao, H. L., and Hou, J.: OH, HO<sub>2</sub>, and OH reactivity during the PMTACS-NY Whiteface

1 Mountain 2002 campaign: Observations and model comparison, *J. Geophys. Res.*, 111,  
2 D10S03, 10.1029/2005JD006126, 2006.

3 Ren, X., Sanders, J. E., Rajendran, A., Weber, R. J., Goldstein, A. H., Pusede, S. E., Browne,  
4 E. C., Min, K.-E., and Cohen, R. C.: A relaxed eddy accumulation system for measuring  
5 vertical fluxes of nitrous acid, *Atmos. Meas. Tech.*, 4, 2093–2103, 10.5194/amt-4-2093-2011,  
6 2011.

7 Rutter, A. P., Malloy, Q. G. J., Leong, Y. J., Gutierrez, C. V., Calzada, M., Scheuer, E., Dibb,  
8 J. E. and Griffin, R. J.: The reduction of HNO<sub>3</sub> by volatile organic compounds emitted by  
9 motor vehicles, *Atmos. Environ.*, 87, 200–206, doi:10.1016/j.atmosenv.2014.01.056, 2014.

10 Salmon, R. A., Bauguitte, S. J. B., Bloss, W., Hutterli, M. A., Jones, A. E., Read, K., and  
11 Wolff, E. W.: Measurement and interpretation of gas phase formaldehyde concentrations  
12 obtained during the CHABLIS campaign in coastal Antarctica, *Atmos. Chem. Phys.*, 8, 4085-  
13 4093, 10.5194/acp-8-4085-2008, 2008.

14 Sander, S. P., and Peterson, M. E.: Kinetics of the Reaction HO<sub>2</sub>+NO<sub>2</sub>+M = HO<sub>2</sub>NO<sub>2</sub>+M, *J.*  
15 *Phys. Chem.*, 88, 1566-1571, 10.1021/j150652a025, 1984.

16 Scharko, N. K., Berke, A. E. and Raff, J. D.: Release of Nitrous Acid and Nitrogen Dioxide  
17 from Nitrate Photolysis in Acidic Aqueous Solutions, *Environ. Sci. Technol.*, **48**, 11991-  
18 12001, doi:10.1021/es503088x, 2014.

19 Sörgel, M., Trebs, I., Serafimovich, A., Moravek, A., Held, A. and Zetzsch, C.: Simultaneous  
20 HONO measurements in and above a forest canopy: Influence of turbulent exchange on  
21 mixing ratio differences, *Atmos. Chem. Phys.*, 11(2), 841–855, doi:10.5194/acp-11-841-2011,  
22 2011a.

23 Sörgel, M., Regelin, E., Bozem, H., Diesch, J.-M., Drewnick, F., Fischer, H., Harder, H.,  
24 Held, A., Hosaynali-Beygi, Z., Martinez, M. and Zetzsch, C.: Quantification of the unknown  
25 HONO daytime source and its relation to NO<sub>2</sub>, *Atmos. Chem. Phys.*, 11(20), 10433–10447,  
26 doi:10.5194/acp-11-10433-2011, 2011b.

27 Sörgel, M., Trebs, I., Wu, D. and Held, A.: A comparison of measured HONO uptake and  
28 release with calculated source strengths in a heterogeneous forest environment, *Atmos. Chem.*  
29 *Phys.*, 15(16), 9237–9251, doi:10.5194/acp-15-9237-2015, 2015.

1 Steinbacher, M., Zellweger, C., Schwarzenbach, B., Bugmann, S., Buchmann, B., Ordonez,  
2 C., Prevot, A. S. H., and Hueglin, C.: Nitrogen oxide measurements at rural sites in  
3 Switzerland: Bias of conventional measurement techniques, *J. Geophys. Res.*, 112, D11307,  
4 10.1029/2006jd007971, 2007.

5 Stemmler, K., Ammann, M., Donders, C., Kleffmann, J., and George, C.: Photosensitized  
6 reduction of nitrogen dioxide on humic acid as a source of nitrous acid, *Nature*, 440, 195-198,  
7 10.1038/nature04603, 2006.

8 Stemmler, K., Ndour, M., Elshorbany, Y., Kleffmann, J., D'Anna, B., George, C., Bohn, B.,  
9 and Ammann, M.: Light induced conversion of nitrogen dioxide into nitrous acid on  
10 submicron humic acid aerosol, *Atmos. Chem. Phys.*, 7, 4237-4248, 2007.

11 Stone, D. and Rowley, D. M., Kinetics of the Gas Phase HO<sub>2</sub> Self-Reaction: Effects of  
12 Temperature, Pressure, Water and Methanol Vapours, *Phys. Chem. Chem. Phys.*, 7, 2156 –  
13 2163, 2005.

14 Stutz, J., Alicke, B., and Neftel, A.: Nitrous acid formation in the urban atmosphere: Gradient  
15 measurements of NO<sub>2</sub> and HONO over grass in Milan, Italy, *J. Geophys. Res.*, 107, 8192,  
16 10.1029/2001jd000390, 2002.

17 Su, H., Cheng, Y. F., Cheng, P., Zhang, Y. H., Dong, S., Zeng, L. M., Wang, X., Slanina, J.,  
18 Shao, M., and Wiedensohler, A.: Observation of nighttime nitrous acid (HONO) formation at  
19 a non-urban site during PRIDE-PRD2004 in China, *Atmos. Environ.*, 42, 6219-6232,  
20 10.1016/j.atmosenv.2008.04.006, 2008a.

21 Su, H., Cheng, Y. F., Shao, M., Gao, D. F., Yu, Z. Y., Zeng, L. M., Slanina, J., Zhang, Y. H.,  
22 and Wiedensohler, A.: Nitrous acid (HONO) and its daytime sources at a rural site during the  
23 2004 PRIDE-PRD experiment in China, *J. Geophys. Res. Atmos.*, 113, D14312,  
24 10.1029/2007jd009060, 2008b.

25 Su, H., Cheng, Y., Oswald, R., Behrendt, T., Trebs, I., Meixner, F. X., Andreae, M. O.,  
26 Cheng, P., Zhang, Y., and Pöschl, U.: Soil Nitrite as a Source of Atmospheric HONO and OH  
27 Radicals, *Science*, 333, 1616-1618, 10.1126/science.1207687, 2011.

28 Trebs, I., Lara, L. L., Zeri, L. M. M., Gatti, L. V., Artaxo, P., Slanina, J., Andreae, M. O., and  
29 Meixner, F. X.: Dry and wet deposition of inorganic nitrogen compounds to a tropical pasture  
30 site (Rondonia, Brazil), *Atmos. Chem. Phys.*, 6, 447–469, 2006.

1 Tyndall, G. S., Orlando, J. J., and Calvert, J. G.: Upper Limit for the Rate Coefficient for the  
2 Reaction  $\text{HO}_2 + \text{NO}_2 \rightarrow \text{HONO} + \text{O}_2$ , *Environ. Sci. Technol.*, 29, 202-206,  
3 10.1021/es00001a026, 1995.

4 VandenBoer, T. C., Brown, S. S., Murphy, J. G., Keene, W. C., Young, C. J., Pszenny, A. A.  
5 P., Kim, S., Warneke, C., de Gouw, J. A., Maben, J. R., Wagner, N. L., Riedel, T. P.,  
6 Thornton, J. A., Wolfe, D. E., Dubé, W. P., Öztürk, F., Brock, C. A., Grossberg, N., Lefer, B.,  
7 Lerner, B., Middlebrook, A. M., and Roberts, J. M.: Understanding the role of the ground  
8 surface in HONO vertical structure: High resolution vertical profiles during NACHTT-11, *J.*  
9 *Geophys. Res.*, 118, 10,155–10,171, doi:10.1002/jgrd.50721, 2013.

10 VandenBoer, T. C., Young, C. J., Talukdar, R. K., Markovic, M. Z., Brown, S. S., Roberts, J.  
11 M. and Murphy, J. G.: Nocturnal loss and daytime source of nitrous acid through reactive  
12 uptake and displacement, *Nature Geosci.*, 8(1), 55–60, doi:10.1038/ngeo2298, 2015.

13 Villena, G., Kleffmann, J., Kurtenbach, R., Wiesen, P., Lissi, E., Rubio, M. A., Croxatto, G.,  
14 and Rappenglück, B.: Vertical gradients of HONO,  $\text{NO}_x$  and  $\text{O}_3$  in Santiago de Chile, *Atmos.*  
15 *Environ.*, 45, 3867-3873, 10.1016/j.atmosenv.2011.01.073, 2011.

16 Villena, G., Bejan, I., Kurtenbach, R., Wiesen, P., and Kleffmann, J.: Interferences of  
17 commercial  $\text{NO}_2$  instruments in the urban atmosphere and in a smog chamber, *Atmos. Meas.*  
18 *Tech.*, 5, 149-159, 10.5194/amt-5-149-2012, 2012.

19 Vogel, B., Vogel, H., Kleffmann, J. and Kurtenbach, R.: Measured and simulated vertical  
20 profiles of nitrous acid - Part II. Model simulations and indications for a photolytic source,  
21 *Atmos. Environ.*, 37(21), 2957–2966, doi:10.1016/S1352-2310(03)00243-7, 2003.

22 Whalley, L. K., Blitz, M. A., Desservettaz, M., Seakins, P. W., and Heard, D. E.: Reporting  
23 the sensitivity of laser-induced fluorescence instruments used for  $\text{HO}_2$  detection to an  
24 interference from  $\text{RO}_2$  radicals and introducing a novel approach that enables  $\text{HO}_2$  and certain  
25  $\text{RO}_2$  types to be selectively measured, *Atmos. Meas. Tech.*, 6, 3425-3440, 10.5194/amt-6-  
26 3425-2013, 2013.

27 Whalley, L. K., Stone, D., George, I. J., Mertes, S., van Pinxteren, D., Tilgner, A., Herrmann,  
28 H., Evans, M. J., and Heard, D. E.: The influence of clouds on radical concentrations:  
29 observations and modelling studies of  $\text{HO}_x$  during the Hill Cap Cloud Thuringia (HCCT)  
30 campaign in 2010, *Atmos. Chem. Phys.*, 15, 3289-3301, 2015a.

1 Whalley, L. K., Stone, D., Bandy, B., Dunmore, R., Hamilton, J. F., Hopkins, J. R., Lee, J. D.,  
2 Lewis, A. C., and Heard, D. E., Atmospheric OH reactivity in central London: observations,  
3 model predictions and estimates of in situ ozone production, *Atmos. Chem. Phys. Discuss.*,  
4 15, 31247-31286, 2015b.

5 Wong, K. W., Oh, H.-J., Lefer, B. L., Rappenglück, B., and Stutz, J.: Vertical Profiles of  
6 Nitrous Acid in the Nocturnal Urban Atmosphere of Houston, TX, *Atmos. Chem. Phys.*, 11,  
7 3595-3609, doi:10.5194/acp-11-3595-2011, 2011.

8 Wong, K. W., Tsai, C., Lefer, B., Haman, C., Grossberg, N., Brune, W. H., Ren, X., Luke,  
9 W., and Stutz, J.: Daytime HONO vertical gradients during SHARP 2009 in Houston, TX,  
10 *Atmos. Chem. Phys.*, 12, 635-652, 10.5194/acp-12-635-2012, 2012.

11 Wong, K. W., Tsai, C., Lefer, B., Grossberg, N. and Stutz, J.: Modeling of daytime HONO  
12 vertical gradients during SHARP 2009, *Atmos. Chem. Phys.*, 13(7), 3587–3601,  
13 doi:10.5194/acp-13-3587-2013, 2013.

14 Ye, C.; Zhou, X.; Pu, D.; Stutz, J.; Festa, J.; Spolaor, M.; Cantrell, C.; Mauldin, R. L.;  
15 Weinheimer, A.; Haggerty, J. Comment on “Missing Gas-phase Source of HONO Inferred  
16 from Zeppelin Measurements in the Troposphere”, *Science*, 348, 1326-d, 2015.

17 Young, C. J., Washenfelder, R. A., Roberts, J. M., Mielke, L. H., Osthoff, H. D., Tsai, C.,  
18 Pikelnaya, O., Stutz, J., Veres, P. R., Cochran, A. K., Vandenkoer, T. C., Flynn, J., Grossberg,  
19 N., Haman, C. L., Lefer, B., Stark, H., Graus, M., De Gouw, J., Gilman, J. B., Kuster, W. C.  
20 and Brown, S. S.: Vertically resolved measurements of nighttime radical reservoirs in Los  
21 Angeles and their contribution to the urban radical budget, *Environ. Sci. Technol.*, 46(20),  
22 10965–10973, doi:10.1021/es302206a, 2012.

23 Young, D. E., Allan, J. D., Williams, P. I., Green D. C., Harrison, R. M., Yin, J., Flynn, M. J.,  
24 Gallagher, M. W. and Coe, H.: Investigating a two-component model of solid fuel organic  
25 aerosol in London: processes, PM1 contributions, and seasonality, *Atmos. Chem. Phys.*, 15,  
26 2429-2443, 2015.

27 Zhang, N., Zhou, X., Shepson, P. B., Gao, H., Alaghmand, M. and Stirm, B.: Aircraft  
28 measurement of HONO vertical profiles over a forested region, *Geophys. Res. Lett.*, 36(15),  
29 L15820, doi:10.1029/2009GL038999, 2009.

30 Zhang, N., Zhou, X., Bertman, S., Tang, D., Alaghmand, M., Shepson, P. B., and Carroll, M.  
31 A.: Measurements of ambient HONO concentrations and vertical HONO flux above a

1 northern Michigan forest canopy, *Atmos. Chem. Phys.*, 12, 8285-8296, doi:10.5194/acp-12-  
2 8285-2012, 2012

3 Zhou, X., Civerolo, K., Dai, H., Huang, G., Schwab, J., and Demerjian, K.: Summertime  
4 nitrous acid chemistry in the atmospheric boundary layer at a rural site in New York State, *J.*  
5 *Geophys. Res.*, 107, 4590, 10.1029/2001jd001539, 2002.

6 Zhou, X., Gao, H., He, Y., Huang, G., Bertman, S. B., Civerolo, K., and Schwab, J.: Nitric  
7 acid photolysis on surfaces in low-NO<sub>x</sub> environments: Significant atmospheric implications,  
8 *Geophys. Res. Lett.*, 30, 2217, 10.1029/2003gl018620, 2003.

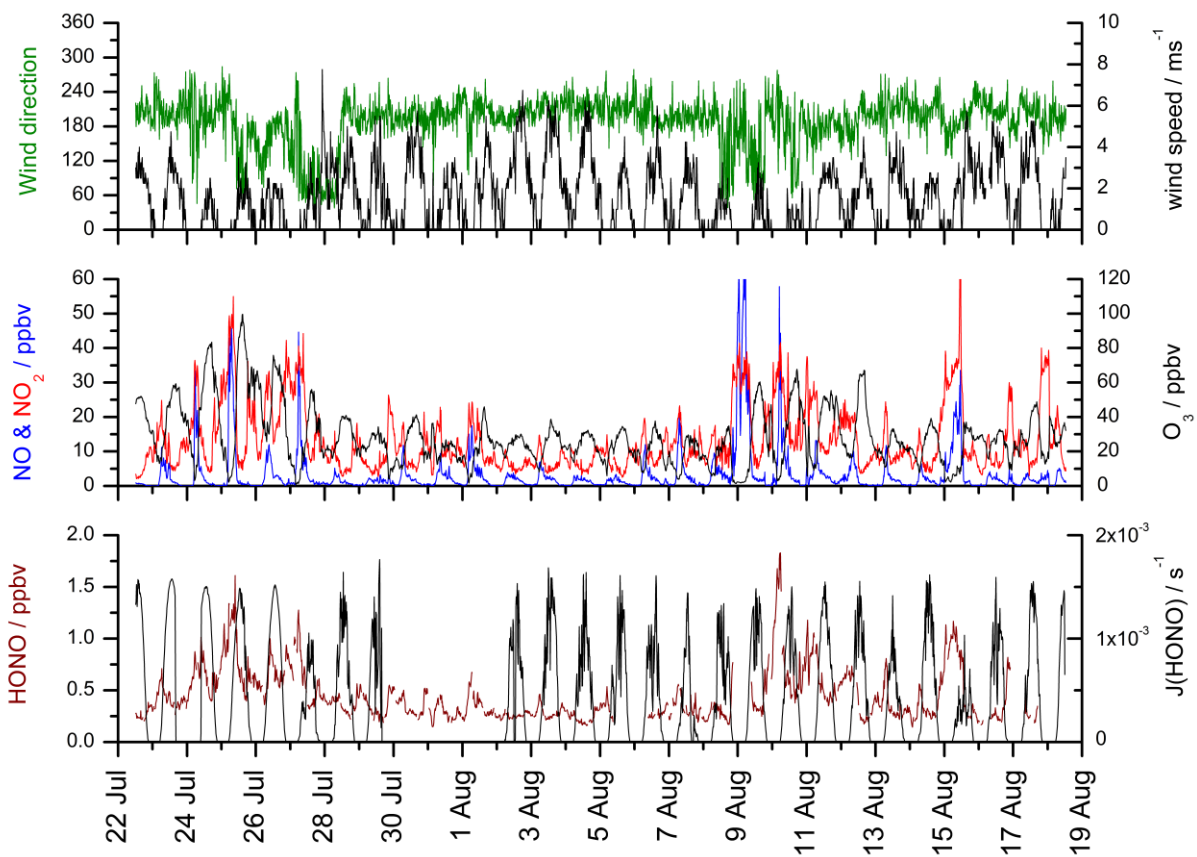
9 Zhou, X., Zhang, N., TerAvest, M., Tang, D., Hou, J., Bertman, S., Alaghmand, M., Shepson,  
10 P. B., Carroll, M. A., Griffith, S., Dusanter, S., and Stevens, P. S.: Nitric acid photolysis on  
11 forest canopy surface as a source for tropospheric nitrous acid, *Nature Geoscience*, 4, 440-  
12 443, doi:10.1038/NGEO1164, 2011.

13 Ziemba, L. D., Dibb, J. E., Griffin, R. J., Anderson, C. H., Whitlow, S. I., Lefer, B. L.,  
14 Rappenglück, B. and Flynn, J.: Heterogeneous conversion of nitric acid to nitrous acid on the  
15 surface of primary organic aerosol in an urban atmosphere, *Atmos. Environ.*, 44(33), 4081-  
16 4089, doi:10.1016/j.atmosenv.2008.12.024, 2010.

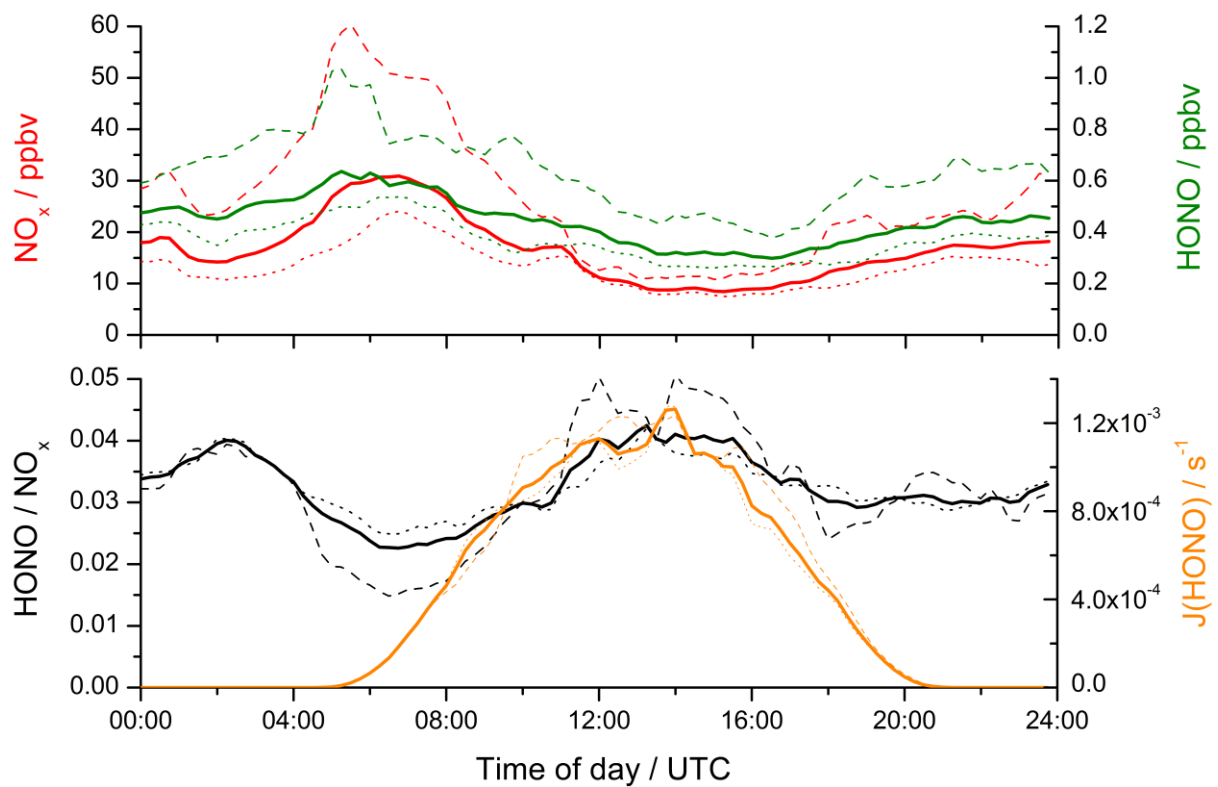
17  
18

1 Table 1. Correlation coefficients ( $r^2$ ) for plots between various species measured during  
 2 ClearfLo (and their products), using  $j(NO_2)$  as a proxy for radiation, and the missing HONO  
 3 source from the model (using the model with all additional sources). The species used were  
 4 chosen using the method described in the text. SA = total aerosol surface area. See  
 5 supplementary material figure S1 for plots.

Species	$r^2$ for correlation vs missing HONO
<b>j(NO<sub>2</sub>)</b>	0.5394
<b>H<sub>2</sub>O</b>	0.0004
<b>NO</b>	0.0270
<b>NO<sub>2</sub></b>	0.0001
<b>Temp</b>	0.3557
<b>HNO<sub>3 ads.</sub></b>	0.0966
<b>OH</b>	0.2745
<b>HO<sub>2</sub></b>	0.1925
<b>RO<sub>2</sub></b>	0.2763
<b>k(OH)</b>	0.0001
<b>NO<sub>3<sup>-</sup> aero.</sub></b>	0.0006
<b>NH<sub>4<sup>+</sup> aero.</sub></b>	0.0007
<b>aerosol surface area (SA)</b>	0.0001
<b>j(NO<sub>2</sub>) × H<sub>2</sub>O</b>	0.5981
<b>j(NO<sub>2</sub>) × NO<sub>2</sub></b>	0.6960
<b>j(NO<sub>2</sub>) × T</b>	0.6276
<b>j(NO<sub>2</sub>) × k(OH)</b>	0.6781
<b>j(NO<sub>2</sub>) × NH<sub>4<sup>+</sup></sub></b>	0.5829
<b>j(NO<sub>2</sub>) × HNO<sub>3 ads.</sub></b>	0.4356
<b>H<sub>2</sub>O × HNO<sub>3 ads.</sub></b>	0.1044
<b>H<sub>2</sub>O × OH</b>	0.3378
<b>H<sub>2</sub>O × RO<sub>2</sub></b>	0.2899
<b>H<sub>2</sub>O × NO<sub>3<sup>-</sup> aero.</sub></b>	0.0006
<b>NO × HNO<sub>3</sub></b>	0.1276
<b>NO × OH</b>	0.2791
<b>NO × HO<sub>2</sub></b>	0.2580
<b>NO<sub>2</sub> × OH</b>	0.3867
<b>temp × OH</b>	0.3952
<b>OH × k(OH)</b>	0.3497
<b>OH × NH<sub>4<sup>+</sup> aero.</sub></b>	0.3888
<b>HO<sub>2</sub> × k(OH)</b>	0.1941
<b>RO<sub>2</sub> × k(OH)</b>	0.2819
<b>j(NO<sub>2</sub>) × NO<sub>2</sub> × T</b>	0.7262
<b>j(NO<sub>2</sub>) × T × k(OH)</b>	0.7069
<b>j(NO<sub>2</sub>) × NO<sub>2</sub> × k(OH)</b>	0.6594
<b>NO × HNO<sub>3 ads.</sub> × OH</b>	0.4085
<b>NO × HNO<sub>3 ads.</sub> × HO<sub>2</sub></b>	0.2916
<b>NO × HNO<sub>3 ads.</sub> × RO<sub>2</sub></b>	0.3198
<b>j(NO<sub>2</sub>) × H<sub>2</sub>O × T × k(OH)</b>	0.7280



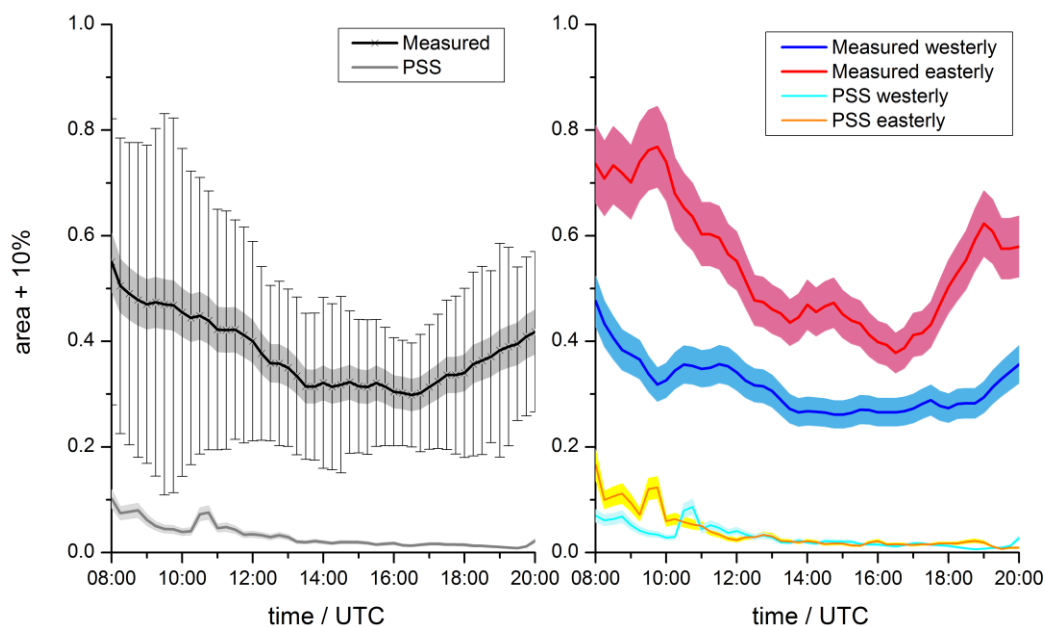
1  
 2 Figure 1. Time series of selected data from the ClearfLo intensive operation period (July and  
 3 August 2012). The top panel shows wind speed (black) and wind direction (green); the middle  
 4 panel shows NO (blue), NO<sub>2</sub> (red) and O<sub>3</sub> (black); and the bottom panel shows HONO (dark  
 5 red) and j(HONO) (black). All data is 15 minute averaged and plotted as UTC (local time - 1  
 6 hour).



1  
2  
3  
4  
5  
6  
7  
8  
9

Figure 2. Average diurnal profiles of selected data from the IOP. The top panel shows total NO<sub>x</sub> (red) and HONO (green) and the bottom panel shows  $j(HONO)$  (orange) and the HONO / NO<sub>x</sub> ratio (black). Profiles were generated by binning all data in a 15 minute time period together. For each, the solid line is the total of all days, the dashed line is data from easterly conditions and the dotted line data from westerly conditions (see text for dates).

1

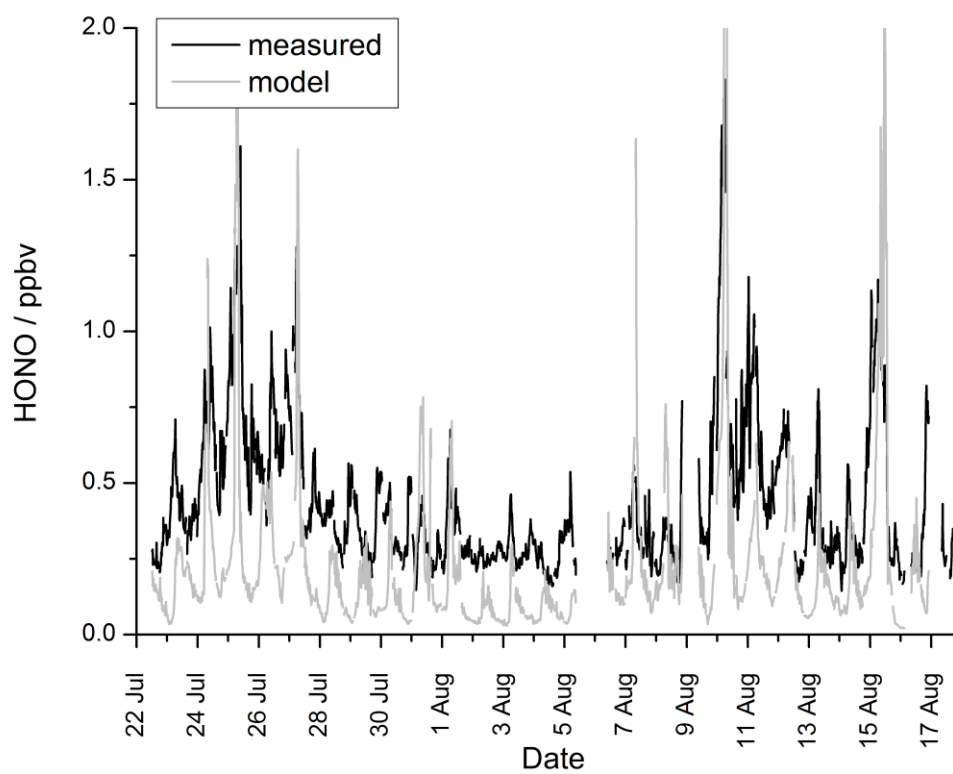


2

3 Figure 3. Average diurnal profiles (daylight hours) of measured (black) and photostationary  
4 state (PSS) calculated (grey) HONO (left panel). The shaded area represents instrumental  
5 ( $\pm 10\%$ ) and model ( $\pm 17\%$ ) error, the bars represent the standard deviation of the  
6 measurements. The right panel shows averaged diurnal profiles of measured and PSS HONO  
7 divided into easterly (red / orange) and westerly (blue / cyan) conditions. The shaded area  
8 represents the measurement ( $\pm 10\%$ ) and PSS ( $\pm 17\%$ ) error.

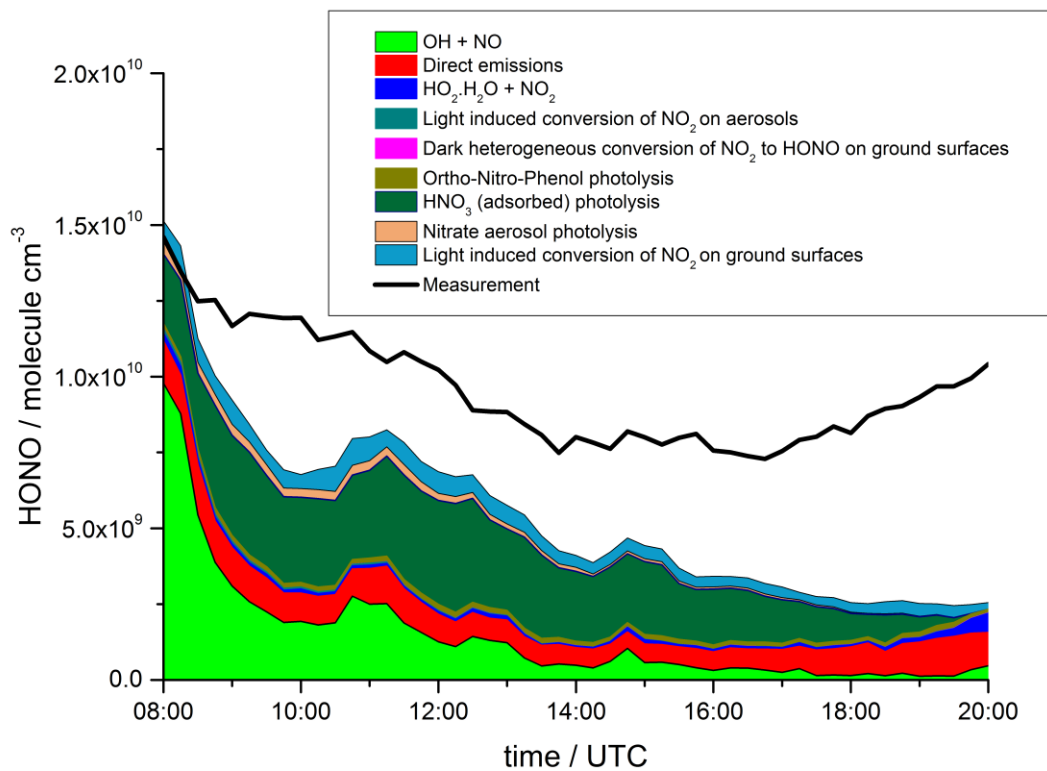
9

10

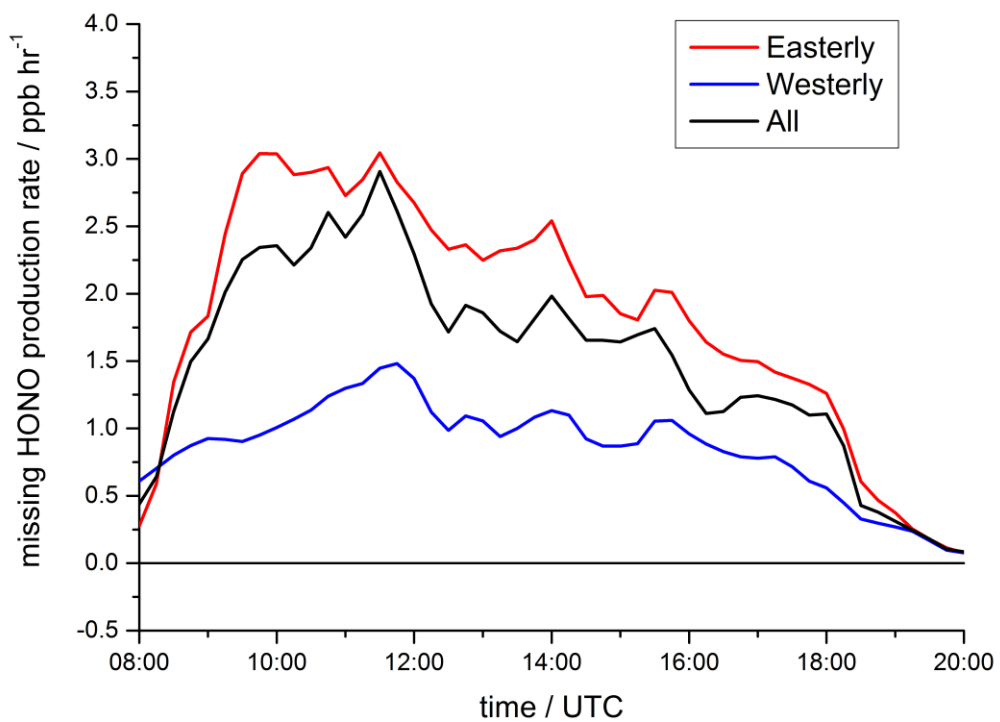


1  
2 Figure 4. Time series of measured (black) and model calculated (grey) HONO during the IOP.  
3 The model was based on the Master Chemical Mechanism (MCM v3.2), see text for details.

4  
5  
6

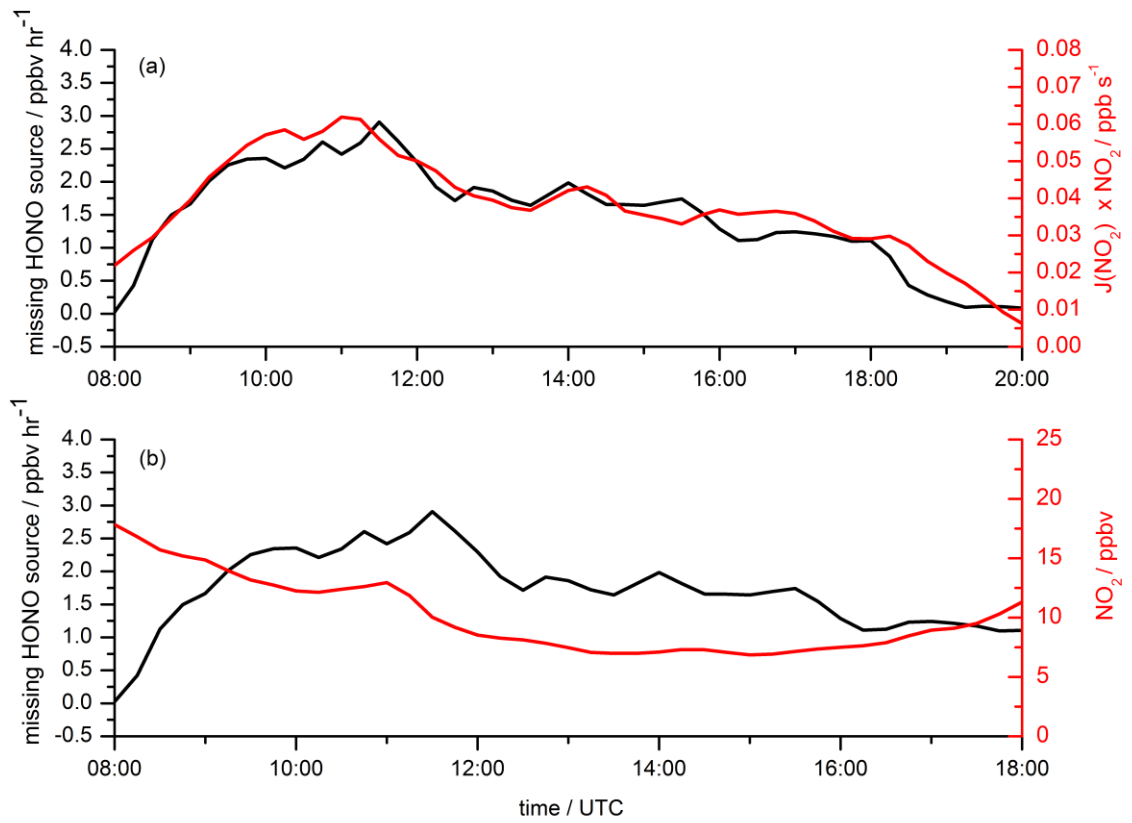


1  
 2 Figure 5. Average daytime diurnal profile of the modelled HONO from different sources  
 3 shown as a compound area plot, as described in section 3.3 of the text. Also plotted (black  
 4 trace) is the measured HONO.  
 5



1  
 2 Figure 6. Average daytime diurnal profile of the ‘missing’ HONO production rate (in ppb hr<sup>-1</sup>), defined as the rate of HONO production required to reproduce the measurements in the  
 3 model. The black trace shows average of all data, the red trace shows the average of data from  
 4 easterly conditions and the blue trace shows the average of data from westerly conditions.  
 5

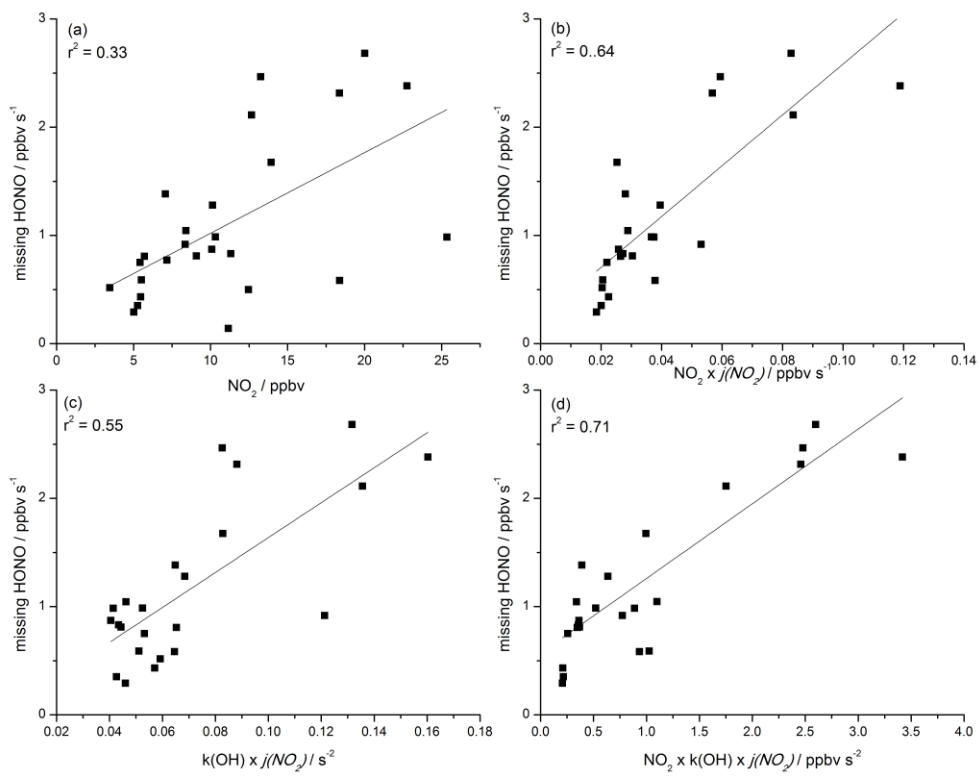
6  
 7



1

2 Figure 7. Average diurnal profiles of the missing HONO source (black traces) plotted with (as  
 3 red traces) (a)  $\text{NO}_2 \times j(\text{NO}_2)$  and (b)  $\text{NO}_2$ .

4

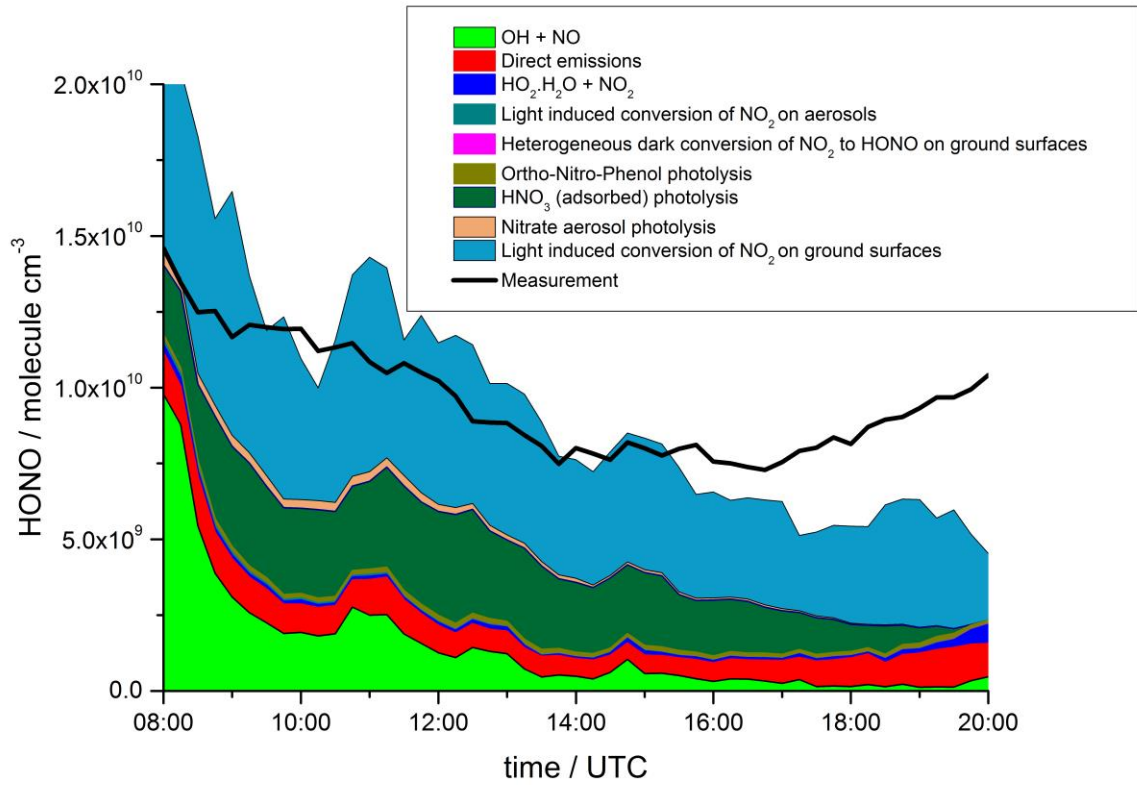


1

2 Figure 8. Daytime averaged (08:00 – 19:00) missing HONO source plotted against (a)  $\text{NO}_2$ ,  
 3 (b)  $\text{NO}_2 \times j(\text{NO}_2)$ , (c)  $k(\text{OH}) \times j(\text{NO}_2)$ , (d)  $\text{NO}_2 \times k(\text{OH}) \times j(\text{NO}_2)$ .

4

5



1

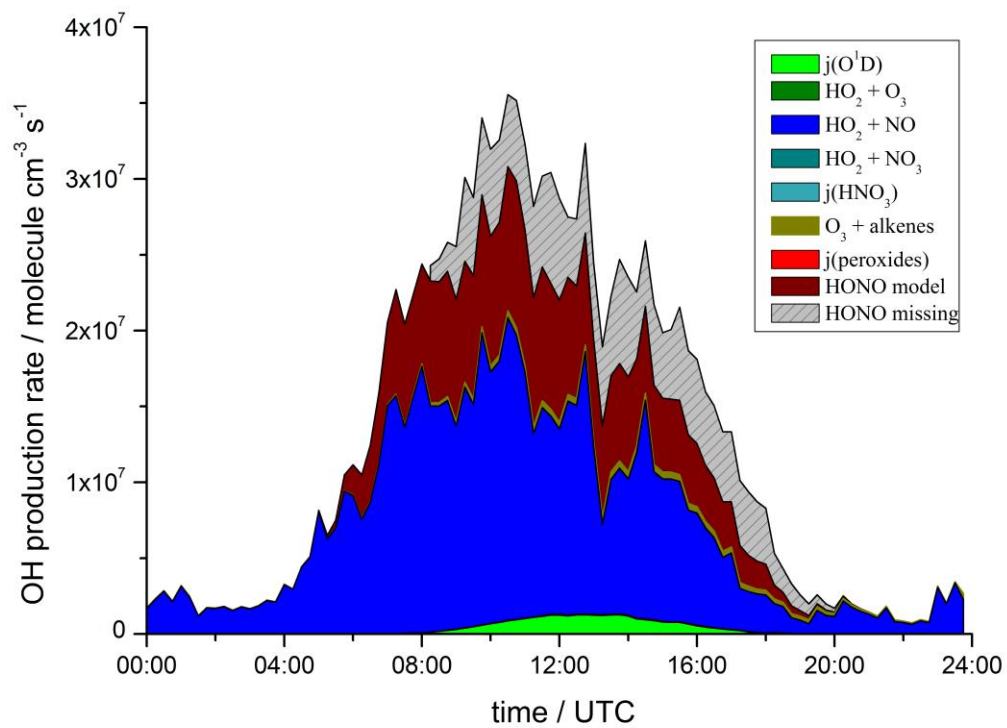
2 Figure 9. Average daytime diurnal profile of the modelled HONO from different sources  
 3 shown as a compound area plot, as described in section 3.3 of the text, showing the result of  
 4 increasing the reactive uptake coefficient of the light enhanced conversion of NO<sub>2</sub> on ground  
 5 surfaces (see text for details). Also plotted (black trace) is the measured HONO.

6

7

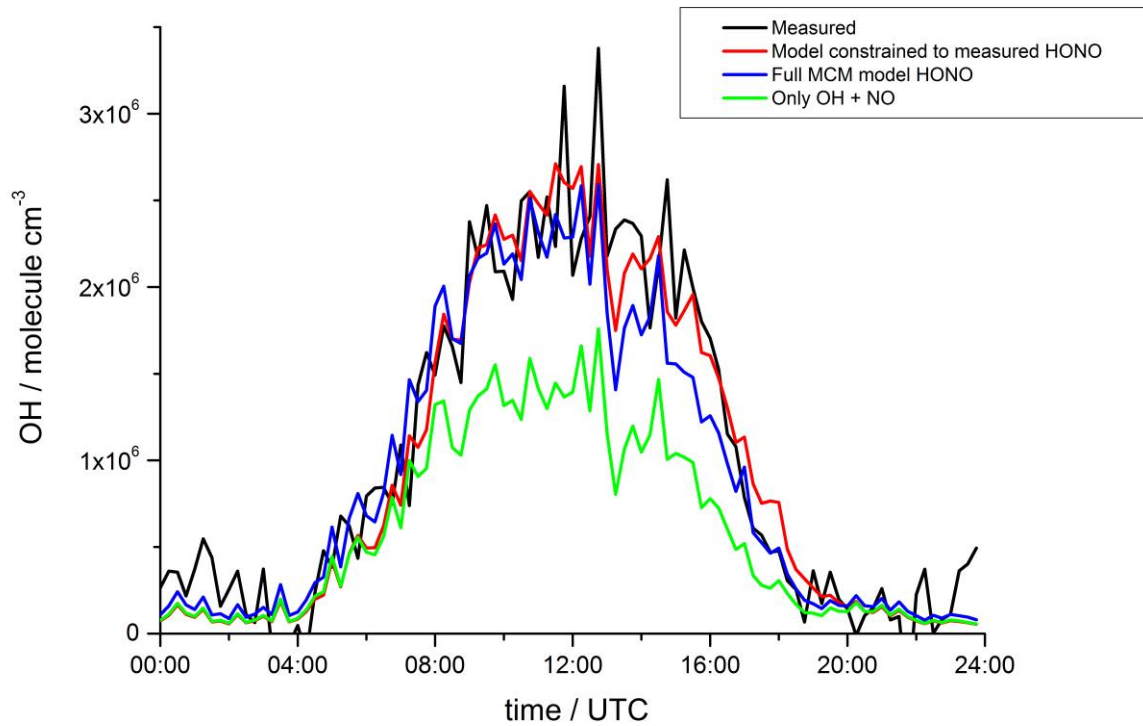
8

1



2  
3 Figure 10. Average diurnal profile of gross OH production rates from different initiation and  
4 propagation sources calculated by the model.

1



2

3 Figure 11. Average diurnal profile of OH, showing measured (black), modelled unconstrained  
4 to HONO with only NO + OH as a HONO sources (green), modelled unconstrained to  
5 HONO including additional HONO sources (blue – see text for details) and model  
6 constrained to measured HONO (red).